

---

# Chapter 21

# Ground Penetrating Radar

---

## David Daniels

*ERA Technology*

---

### 21.1 INTRODUCTION

---

The terms *ground penetrating radar (GPR)*, *ground probing radar*, *subsurface radar*, or *surface penetrating radar (SPR)* refer to a radar-based electromagnetic technique designed primarily for the location of objects or interfaces buried beneath the Earth's surface or located within a visually opaque structure. GPR is a successful example of the exploitation of ultrawideband radar and typically a GPR with a range of 1 m would operate over the range 0.3 GHz to 3.3 GHz.

Although GPR has many similarities to radar systems, there are some key differences, which need to be appreciated when comparing them with conventional radar systems. GPR systems are a special class of ultrawideband (UWB) radar system and can radiate energy in the range of frequencies from a few MHz up to 10 GHz with a bandwidth of up to a decade, but more usually 2–3 octaves. The typical average radiated power, integrated over the band of interest, may be in the order of a milliwatt, but the power per Hz may be as low as picowatts.

GPR is usually operated so that the target, which is within a lossy dielectric, is only a few wavelengths from the aperture of antenna. The total path losses within a few wavelengths may reach 100 dB or more depending on the material. Many GPR systems operate in a region where the wavelengths radiated are greater or in the same order of magnitude as the target dimensions. Thus, GPR operates between the Rayleigh region and Mie or resonance region of the target dimensions. This is very different from conventional radar systems where the target dimensions are much larger than the wavelength of the incident radiation, i.e., the optical region.

The technology of GPR is largely applications-oriented and the overall design philosophy, as well as the hardware, is usually dependent on the target type and the material of the target and its surroundings. GPR is vulnerable to extremely high levels of clutter at short ranges and this, rather than signal/noise recovery, is its major technical challenge. The system to be specified should take this into account. All these aspects pose special design problems for GPR, which is described in detail by Daniels.<sup>1</sup> This chapter is a summary of that material and is referenced by courtesy of the IEE.

A typical GPR system is shown in Figure 21.1 and consists of a pair of antennas, one for transmit and one for receive, connected to the transmitter receiver and processor and contained within a sealed enclosure, a battery and control processor, and display unit. The wheels drive a shaft encoder that triggers data acquisition and hence the display that is synchronised to the movement of the system. An example of the display,

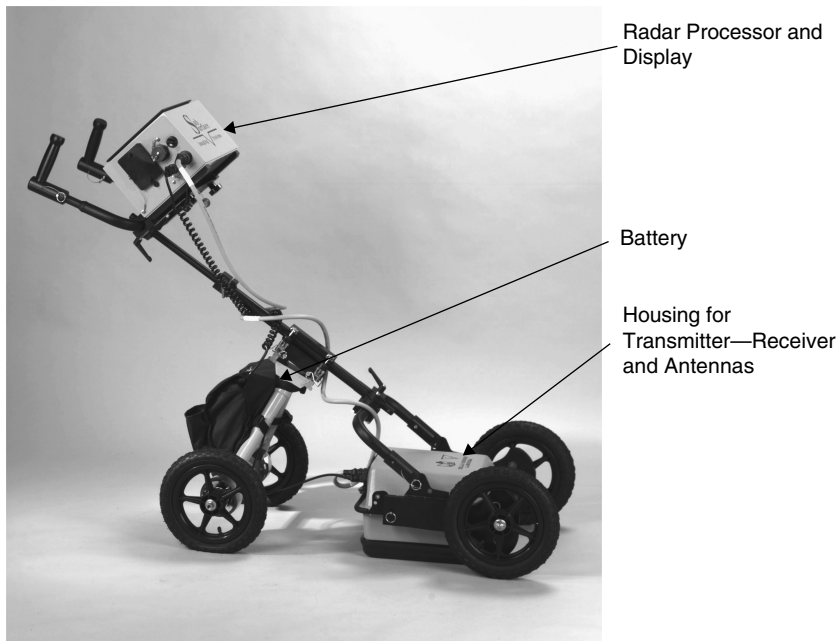


**FIGURE 21.1** Typical GPR system (*Courtesy US Radar*)

which takes the form of a cross section of the ground surveyed by the GPR, is shown in Figure 21.2. The horizontal scale is 10 cm per marker and the vertical scale is time in nanoseconds (51 ns). An explanation of the image is provided later in this chapter.

GPR system design can be classified into two groups. GPR systems that transmit an impulse and receive the reflected signal from the target using a sampling receiver can be considered to operate in the time domain. GPR systems that transmit individual frequencies in a sequential manner and receive the reflected signal from the target using a frequency conversion receiver can be considered to operate in the frequency domain.

The first use of electromagnetic signals to determine the presence of remote terrestrial metal objects is generally attributed to Hülsmeyer in 1904, but the first description of their use for location of buried objects appeared six years later in a German patent by Leimbach and Löwy. The work of Hülsenbeck in 1926 appears to be the first use of pulsed techniques to determine the structure of buried features. He noted that any

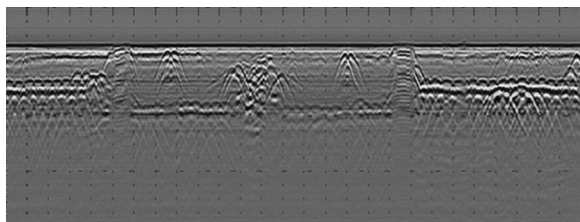


**FIGURE 21.2** Typical display from GPR

dielectric variation, not necessarily involving conductivity, would also produce reflections and that the technique, through the easier realization of directional sources, had advantages over seismic methods. Pulsed techniques were developed from the 1930s onward as a means of probing to considerable depths in ice (Stenson<sup>2</sup> and Evans<sup>3</sup>); in fresh water and salt deposits (Unterberger<sup>4</sup>); in desert sand and rock formations (Kadaba<sup>5</sup> and Morey<sup>6</sup>). Probing of rock and coal was also investigated by Cook<sup>7,8</sup> as well as Roe,<sup>9</sup> although the higher attenuation in the latter material meant that depths greater than a few meters were impractical. Nilsson<sup>10</sup> gives a more extended account of the history of GPR and its growth up to the mid-1970s. From the 1970s, the range of applications has been expanding steadily, and now includes those given in Table 21.1. Purpose-built equipment for each of these applications has been developed, and the user now has a better choice of equipment and techniques.

GPR has advanced rapidly as a result of a variety of applications, but as the requirements have become more demanding, so the equipment, techniques, and data processing methods have been developed and refined.

A GPR transmits a regular sequence of low-power pulses of electromagnetic energy into the material or ground and then receives and detects the weak reflected signal from the buried target. The energy is in the form of either a very short duration impulse, a sweep over a range of frequencies, radiation of noise over a defined band, or a pseudorandom coded sequence of pulses. Most GPR systems, all of which need to comply with the relevant national and international regulations regarding radio transmitters, operate within the range of frequencies from 10 MHz to 10 GHz and can have a bandwidth of several GHz. The FCC requirement for UWB limits the radiated power to  $-41 \text{ dBm Hz}^{-1}$ . The topic of radar system design is covered in many texts and useful information will be found in the following references: Daniels<sup>11,12</sup> Cook and Bernfeld,<sup>13</sup> Skolnik,<sup>14</sup> Nathanson,<sup>15</sup> Wehner,<sup>16</sup> Galati,<sup>17</sup> and Astanin and Kostylev.<sup>18</sup>

The buried target can be a conductor, a dielectric, or combinations of both. The surrounding host material can be soil, earth materials, wood, rocks, ice, fresh water, or manmade materials such as concrete or brick. A typical GPR achieves a range of up to a few meters, but some special systems can penetrate up to hundreds of meters or even kilometers. A few GPR systems have been operated from aircraft and from satellites to image geological features buried beneath the Saharan deserts as well as measuring the depth of the Moon and features on Mars or comets. The range of the GPR in the ground is limited because of the absorption the signal undergoes, while it travels on its two-way path through the ground material. GPR works well through materials such as granite, dry sand, snow, ice, and fresh water, but will not penetrate certain clays that

**TABLE 21.1** Main Applications of GPR

---

Archaeological investigations
Bridge deck analysis
Detection of buried mines (anti-personnel and anti-tank)
Forensic investigations (detecting buried bodies)
Geophysical investigations
Pipes and cable detection
Rail track and bed inspection
Road condition survey
Snow, ice, and glacier

---

are high in salt content or salt water because of the high absorption of electromagnetic energy of such materials. For comparison, the total two-way path loss from Earth to the Moon using a 1 GHz radar would be greater than 200 dB for a range of 356,400 km and a target radar cross section in the order of  $10^{12} \text{ m}^2$ , whereas a GPR radar often encounters a path loss in excess of 70 dB for ranges of less than a meter.

In air, the GPR signal travels at the speed of light, but is slowed down in ground materials by their dielectric constant; hence, true range needs calibrating for each material. GPR will not penetrate metal because of the latter's conductivity.

There are now a number of commercially available equipments, and the technique is gradually developing in scope and capability. Many GPR systems are mobile and mounted on wheels or skids to be moved by hand, but systems can be used on vehicles for rapid survey by means of an array of antennas. Other GPR systems are designed to be inserted into boreholes to provide images of the intervening rock. Typical GPR system attributes are given in Table 21.2.

Most GPR systems use separate, man-portable, transmit and receive antennas, which are placed on the surface of the ground and moved in a known pattern over the surface of the ground or material under investigation, and an image can be generated, in real time, on a display either in grey scale or in color. By systematically surveying the area in a regular grid pattern, a radar image of the ground can be built up. GPR images are displayed either as two-dimensional representations, using horizontal ( $x$  or  $y$ ) and depth ( $z$ ) axes or a horizontal plane representation ( $x, y$ ) at a given depth ( $z$ ) or as a three-dimensional reconstruction. GPR data may be classified as A-scan, B-scan, or C-scan depending on the plane of image (note these are not the same as conventional radar A, B, and C scans). A GPR A-scan is a measurement at a single fixed point in space and is displayed in amplitude ( $y$ ) and range ( $x$ ). A B-scan is a representation usually in grayscale or color-coded image intensity of a plane ( $x, z$  or  $y, z$ ) of scan whereas a C-scan represents a horizontal plane ( $x, y$ ) at a given depth ( $z$ ). Alternatively, the GPR may be designed to provide an audible warning of target presence while the GPR is moved.

The GPR image of a target is very different from its optical image because the wavelengths of the illuminating radiation are similar in dimension to the target. This results in a much lower definition in the GPR image and one that is highly dependent on the propagation characteristics of the ground. The beam pattern of the antenna is widely spread in the dielectric and this degrades the spatial resolution of the image, unless corrected. Refraction and anisotropic characteristics of the ground may also distort the image. For some longer-range systems, synthetic aperture processing techniques are used to optimize the resolution of the image and will be discussed later.

**TABLE 21.2** Characteristics of GPR Systems in a Soil of Relative Dielectric Constant of 9 and Loss Tangent of 0.1

Pulse Duration in ns	Center Frequency in MHz	Range in Meters	Depth Resolution
0.5	2000	<0.25	0.025
1	1000	<0.5	0.05
2	500	<1	0.1
4	250	<2	0.2
8	125	<4	0.4
16	63	<8	0.8
32	31	<16	1.6

Unprocessed GPR images often show “bright spots” caused by multiple internal reflections as well as a distortion of the aspect ratio of the image of the target caused by variations in the velocity of propagation. Symmetrical targets, such as spheres or pipes, cause migration of the reflected energy to a hyperbolic pattern. GPR images can be processed to compensate for these effects, and this is usually carried out offline. A GPR can be designed to detect specific targets such as interfaces in roads, pipes, and cables by means of polarized radiation and localized objects such as cubes, spheres, and cylinders. GPR is capable of detecting features many hundreds of years old; hence, a prospective site should remain unexcavated, prior to survey, so as to preserve its information.

A simplified diagram of the various sources of clutter in a GPR environment is given in Figure 21.3, and it can be seen that separation of the various signals is the key to identifying the wanted signal.

Inevitably there have been some claims for GPR capability that are simply outside the realms of known physics, and these seem to have been seized on by some sections of the media. A claim was made that a particular GPR and its operator could detect targets the size of golf balls at a depth of eight meters. Clearly, the wavelengths capable of propagating to eight meters in soil would be so much larger than a golf ball-sized target that the radar cross-sectional area of the latter would fade into insignificance, even noise. The persuasiveness of the claimant and the lack of understanding of basic physics on the part of some potential users enabled this kind of claim to be seriously considered. Claims were made that a GPR had been developed “that can provide three-dimensional images of objects up to 45.7 meters below the surface of land and sea. Such a device would allow verifiers to identify underground weapons facilities, like those of concern in Libya, Iraq, and North Korea. The underwater detection capability could also be used to verify treaties dealing with submarines and nuclear weapons positioned on the seabed.” How well

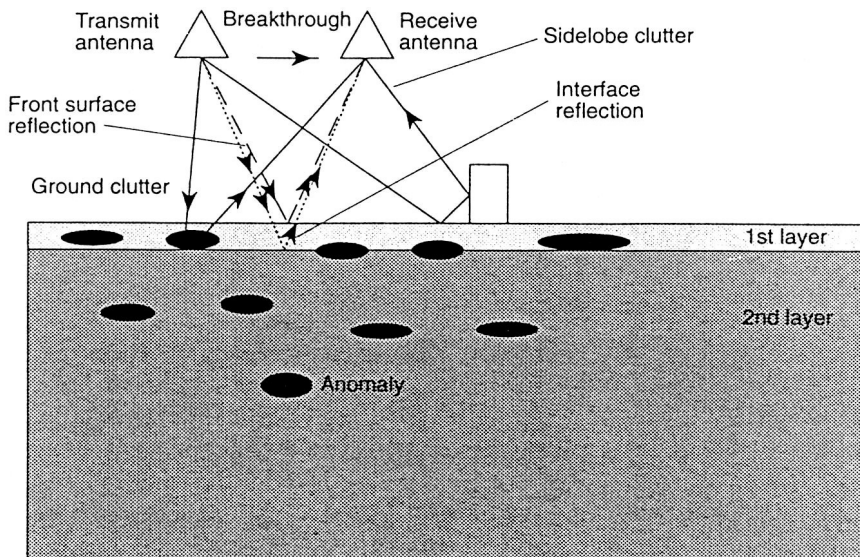


**FIGURE 21.3** General system operation of GPR showing targets and sources of clutter (*Courtesy IEE*)

GPR would propagate through seawater is an interesting question given the known attenuation of seawater at radar frequencies. A careful analysis of some of the claims about the same radar was published by Tuley<sup>19</sup> and is interesting reading.

## 21.2 PHYSICS OF PROPAGATION IN MATERIALS

---

**Introduction.** Conventional radar systems are generally not significantly affected by the propagation characteristics of the medium the radar signals travel through, apart from rain, absorption spectra of the atmosphere, or ionized atmospheric layers. This is definitely not the case with GPR where the transmission medium may be non-isotropic, high dielectric and high loss, and may be layered. Therefore, an understanding of soil and material propagation characteristics is important, and this section describes the key features of the physics of propagation in materials.

Maxwell's equations are the foundation for the consideration of the propagation of electromagnetic waves. In free space, the magnetic susceptibility and electric permittivity are constants, that is, they are independent of frequency and the medium is not dispersive. In a dielectric with a zero loss tangent, no losses due to attenuation are encountered, and hence there is no consideration of the attenuation, which occurs in real dielectric media.

If an alternating electric field is applied to a material, the individual molecules will be induced to rotate in an oscillatory manner about an axis through their centers, the inertia of the molecules preventing them from responding instantaneously. Similar translational effects can occur. The polarization produced by an applied field (such as a propagating radar wave) is closely related to the thermal mobility of the molecules and is, therefore, strongly temperature dependent. Note that polarization in this context is different from the polarization of EM waves. In general, the relaxation time (which may be expressed as a relaxation frequency) depends on activation energy, the natural frequency of oscillation of the polarized particles, and on temperature. Relaxation frequencies vary widely between different materials.

For example, maximum absorption occurs at very low frequencies in ice ( $10^3$  Hz), whereas it takes place in the microwave region in water ( $10^6$  Hz– $10^{10}$  Hz); thus, the effects of this phenomenon can have a direct bearing upon the dielectric properties of materials at the frequencies employed by GPRs, especially if moisture is present within a material. There are a number of other mechanisms, which cause a separation of positively and negatively charged ions resulting in electric polarization. These mechanisms can be associated with ionic atmospheres surrounding colloidal particles (particularly clay minerals), absorbed water, and pore effects, as well as interfacial phenomenon between particles.

The general form of the model that describes the frequency dependence of such systems is the Debye<sup>19</sup> relaxation equation:

$$\epsilon' - i\epsilon'' = \epsilon_{\infty} + \frac{\epsilon_s - \epsilon_{\infty}}{1 + i\omega\tau} \quad (21.1)$$

where

$\epsilon'$  is the real part of the dielectric permittivity,

$\epsilon'$  = real part of the dielectric permittivity

$\epsilon''$  = imaginary part of the dielectric permittivity

$\epsilon_{\infty}$  = high frequency limiting value of the permittivity

$\epsilon_s$  = low frequency limiting value of the permittivity

$\omega$  = radian frequency =  $2\pi f$ )

$\tau$  = relaxation time constant

The frequency of maximum movement and loss occurs at  $\omega = 1/\tau$ .

In general, single relaxations are rarely observed in natural systems. Instead, there are distributions of relaxations corresponding to distributions of size scales that influence movement of charge. There are several equations describing such distributed systems, with the most common experimental observations in agreement with the model from Cole and Cole<sup>20</sup>:

$$\epsilon' - i\epsilon'' = \epsilon_\infty + \frac{\epsilon_s - \epsilon_\infty}{1 + (i\omega\tau)^\alpha} \quad (21.2)$$

where  $\alpha$  describes the breadth of the time constant distribution from a single relaxation,  $\alpha = 1$ , to an infinitely broad distribution,  $\alpha = 0$ , with a common process. Different polarization processes may be described by a series of Cole-Cole equations with different values of  $\alpha$  and other parameters.

The electromagnetic properties of a buried target must be different from the surrounding soil or material, and this means that to a first order its relative dielectric constant should be significantly lesser or greater than the host soil. Typically, most soils exhibit a relative dielectric constant, which ranges between 2 to 25. Fresh water has a relative dielectric constant of approximately 80. It should be noted that the ground and surface are quite likely to be inhomogeneous and contain inclusions of other rocks of various size as well as manmade debris. This suggests that the signal to clutter performance of the sensor is likely to be an important performance factor. Clutter may be regarded as any radar return that is not associated with the wanted target and needs to be defined with respect to a particular application.

**Attenuation.** Electromagnetic waves propagating through natural media experience losses, to both the electric (E) or magnetic (H) fields. This causes attenuation of the original electromagnetic wave. Plane waves are good approximations to real waves in many practical situations. More complicated electromagnetic wavefronts can be considered as a superimposition of plane waves, and this method may be used to gain an insight into more complex situations. For most soils of interest in GPR, the magnetic response is weak and need not be considered as a complex quantity, unlike the permittivity and conductivity. However, in certain soil types, such as those derived from volcanic rocks or otherwise high in iron content, full consideration of the magnetic properties is necessary. In the case of lossy dielectric materials, both conduction and dielectric effects cause absorption of electromagnetic radiation.

The electromagnetic material properties that describe such a system are in the complex propagation constant  $\gamma$ :

$$\gamma = ik = \alpha + i\beta \quad (21.3)$$

where  $\gamma$  = propagation constant

$k$  = wave number ( $2\pi/\lambda$ )

$\alpha$  = attenuation constant [nepers/m]

$\beta$  = phase constant [radians/m]

The field at a distance  $z$  from the source is given by

$$E(z, t) = E_0 \cdot e^{-\alpha z} \cdot e^{j(\omega t - \beta z)} \quad (21.4)$$

The wavelength,  $\lambda$ , in the medium is in meters,

$$\lambda = \frac{2\pi}{\beta} = \frac{\nu}{f} \quad (21.5)$$

where  $f$  is frequency in Hertz.

The losses in such systems are described in terms of tangents of loss angles,  $\delta$ , between electric and magnetic fields. The electrical loss tangent is given by

$$\tan \delta_e = \frac{\epsilon''}{\epsilon'} + \frac{\sigma}{\omega \epsilon'}, \text{ which can be simplified to } \tan \delta_e \approx \frac{\sigma}{\omega \epsilon'} \text{ for low loss materials} \quad (21.6)$$

representing the sum of the charge transport and polarization relaxation losses, and the phase angle between electric field and current density. The skin depth or attenuation length is  $1/\alpha$  [m]; the distance electromagnetic energy travels while being attenuated by  $1/e$  in amplitude. This distance is known as the skin depth,  $d$ , and provides an initial guide to the useful penetration depth of a GPR system although in some media the useful range may be greater.

The individual propagation constants can be written as

$$\alpha = \omega \sqrt{\frac{\mu \epsilon'}{2} \sqrt{1 + \left(\frac{\epsilon''}{\epsilon'}\right)^2} - 1} \quad \beta = \omega \sqrt{\frac{\mu \epsilon'}{2} \sqrt{1 + \left(\frac{\epsilon''}{\epsilon'}\right)^2} + 1}$$

where

$\alpha$  = attenuation factor

$\beta$  = phase constant

and the dimensionless factor  $\epsilon''/\epsilon'$  is more commonly termed the material loss tangent.

This discussion has not considered the electromagnetic and magnetic loss tangent, and these may need to be considered in special cases.

It can be seen from the above expressions that the attenuation constant of a material is, to a first order, linearly related (in  $\text{dBm}^{-1}$ ) to frequency. It is not sufficient to consider only the low frequency conductivity when attempting to determine the loss tangent over the frequency range  $10^7$  to  $10^{10}$  Hz. In the case of a material that is dry and relatively lossless, it may be reasonable to consider that  $\tan \delta_e$  is constant over that frequency range. However, for materials that are wet and lossy such an approximation is invalid. However, there are a number of other factors that influence the effective penetration depth, notably the strength of reflection from the target sought, and the degree of clutter suppression of which the system is capable.

A first order estimate of the various contributions to signal loss can be carried out using the standard radar range equation, although this is only applicable for far-field conditions and thus has restrictions.

$$P_r = \frac{P_t \cdot A \cdot G \cdot \sigma \cdot k}{(4 \cdot \pi \cdot R^2)^2} \cdot e^{-\alpha 2R} \quad (21.7)$$

where

- $P_t$  = transmitted power in watts
- $P_r$  = received power in watts
- $A$  = antenna gain
- $G$  = antenna effective aperture
- $R$  = range in meters
- $\alpha$  = target radar cross section
- $k$  = calibration coefficient

The cumulative losses include the transmission coefficients into the ground; the spreading losses describe the  $R^{-4}$  losses for a target of  $1 \text{ m}^2$ ; and the attenuation losses are for a soil with a  $\epsilon_r$  of 9 and  $\tan \delta$  of 0.1. Fixed losses include the transmission losses into the soil and the effective radar cross section of the target, which comprises its true radar cross section and reflection loss from the target. Note that a conducting reflector will have low return loss whereas a nonconducting reflector will have a high return loss. In Figure 21.4, the calculation has been derived from 1 meter to 10 meters as the radar range equation is not an accurate model in this range less than 1 meter. and the purpose of the explanation is to provide a basic introduction to first order signal estimation.

**Reflection.** In any estimation of received signal level, it is necessary to consider the coefficients of reflection and transmission, as the wave passes through the dielectric to the target and Snell's Laws describe the associated angles of incidence, reflection, transmission, and refraction. Where lossy materials are involved, complex angles of refraction may occur unlike the simple classical case, and polarization and the Stoke's matrix may also be required for oriented high-aspect ratio features like pipes, wires, and fractures.

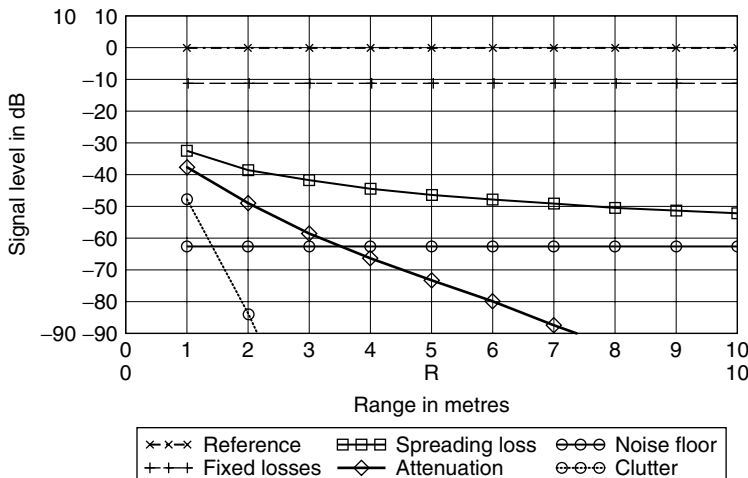


FIGURE 21.4 Losses for GPR signal versus range (Courtesy IEE)

The intrinsic impedance  $\eta$  of a medium is the relationship between the electric field, E, and the magnetic field, H, and is a complex quantity given by

$$\eta = \sqrt{\frac{-j\omega\mu}{\sigma - j\omega\epsilon}} \quad (21.8)$$

At the boundary between two media, some energy will be reflected and the remainder transmitted. The reflected field strength is described by the reflection coefficient,  $r$ :

$$r = \frac{\eta_2 - \eta_1}{\eta_2 + \eta_1} \quad (21.9)$$

where  $\eta_1$  and  $\eta_2$  are the impedances of medium 1 and 2, respectively.

The reflection coefficient has a positive value when  $\eta_2 > \eta_1$ , such as where an air-filled void exists in a dielectric material. The effect on a pulse waveform is to change the phase of the reflected wavelet so that targets with different relative dielectric constants to the host material show different phase patterns of the reflected signal. However, the propagation parameters (relative dielectric constant and loss tangent) of the host material, the geometric characteristics of the target, and its dielectric parameters affect the amplitude of the reflected signal.

**Clutter.** A major difficulty for operation of GPR systems is the presence of clutter within the material. *Clutter* is defined as sources of unwanted reflections that occur within the effective bandwidth and search window of the radar and present as spatially coherent reflectors. The definition of clutter very much depends on the wanted target. The operator of a GPR system searching for pipes may classify the interfaces between road layers as clutter, whereas the operator of a system measuring road layer thickness might consider pipes and cables as sources of clutter. Careful definition and understanding are critically important in selecting and operating the best system and processing algorithms. Clutter can completely obscure the buried target and a proper understanding of its source and impact on the radar is essential.

**Polarization.** A complete description of the radar scattering cross section of a target includes a description of its polarization scattering characteristics (not the same as molecular polarization). The polarizing properties of targets are described by the Stokes parameters, and the polarization coordinates can be represented on the Poincare Sphere. All of these are well described in standard texts on optics and electromagnetic theory. In summary, these descriptions allow the state of an electromagnetic wave to be described in terms of linear, elliptical, and circular polarization (left-handed or right-handed). It is well known that linear targets such as wires act as depolarizing features and that a linearly polarized crossed dipole antenna rotated about an axis normal to a linear target such as a wire or pipe produces a sinusoidal variation in received signal. However, the null points are a distinct disadvantage, because the operator is required to make two separate, axially rotated measurements at every point to be sure of detecting pipes at unknown orientations. An attractive technique is to radiate a circularly polarized wave, which automatically rotates the polarized vector in space and hence removes the direction of signal nulls. These techniques can be used to discriminate in favor of the target. For example, a right-handed circularly polarized (RHCP) wave will be reflected as a left-handed circularly

polarized (LHCP) wave from a planar surface, but some proportion of RHCP will be reflected from a thin pipe or wire. This enables the ground-surface reflection to be reduced while enhancing that from the thin pipe or wire.

**Velocity.** The velocity of propagation of electromagnetic waves in free space is approximately  $3 \times 10^8 \text{ ms}^{-1}$  but slows in a material depending on its relative permittivity and relative magnetic permeability. The velocity of propagation of electromagnetic waves in a soil with a value for  $\epsilon_r$  of 9 would be slowed to  $1 \times 10^8 \text{ ms}^{-1}$ . The time to a target at a range of 1 meter is, therefore, 20 ns, and GPR systems operate at time ranges between a few nanoseconds up to 200 ns, although some systems for probing through ice may use ranges up to several tens of milliseconds.

In general, it is not possible to make a reliable estimate of propagation velocity or relative permittivity in a medium from a single measurement without trial holes (inserting a probe into a predrilled hole) or other supplementary information. Even in the case where a measurement is carried out at one location, it is often found that significant variations in velocity will occur within comparatively short distances from the original location. This can lead to significant errors in the estimation of depths of reflectors. One procedure that overcomes this limitation is known as common depth point surveying, which utilizes two antennas in bistatic operation at a number of transmit and receive positions.

The velocity of propagation is given by  $v = (\mu_o \mu_r \epsilon_o \epsilon_r)^{-1/2}$ , hence in a material with  $\mu_r = 1$ , the velocity becomes  $v = c/(\epsilon_r)^{1/2}$ .

The phase velocity is given by  $v = \omega/\beta$  and as

$$\beta = \omega \sqrt{\frac{\mu \epsilon'}{2} \left( \sqrt{1 + \left( \frac{\epsilon''}{\epsilon'} \right)^2} + 1 \right)} \quad (21.10)$$

The phase velocity is also dependent on the factor  $\epsilon''/\epsilon'$ , which is also  $\tan \delta$ .

It is also possible to derive velocity from multiple measurements scanning over a target, but this works well only in relatively uncluttered situations where the media has no anisotropic characteristics.

**Dispersion.** The frequency dependent nature of the dielectric properties of the material causes the phase velocity of the component frequencies of a wideband signal to suffer differential propagation values. Hence, there will be variation in the velocity of propagation with frequency. Dielectrics exhibiting this phenomenon are termed dispersive. In this situation, the different frequency components within a broadband radar pulse would travel at slightly different speeds, causing the pulse shape to change with time. However, the propagation characteristics of octave band radar signals in most earth materials remain largely unaffected by dispersion. In many instances, the potential variation in the velocity of wave propagation over the frequency range of interest is small and can be ignored.

**Depth Resolution.** For traditional radar systems, it is accepted that two identical targets can be separated in range if they are 0.8 of a pulse width apart. In optics, Lord Rayleigh proposed that the resolving power of an instrument is when the principal intensity of one component coincides with the first intensity minimum of the other component. Many GPR pulses take the form of a Ricker wavelet (the second differential of a gaussian impulse), and an example of two pulses from targets is shown in Figure 21.5 where both the impulses and their envelopes are shown. When the targets are closer, as

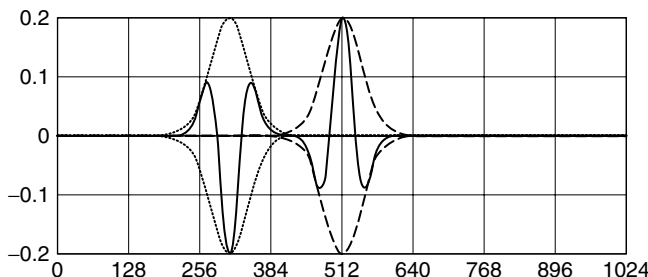


FIGURE 21.5 Two resolved Ricker wavelets

shown in Figure 21.6, although it is possible to distinguish their envelopes, it becomes increasingly difficult to resolve the actual pulses because the signal might be due to a resonance generated by a single target; hence, in the case of pulses with an envelope that has no minima, the 0.8 pulse width resolution criteria may not be optimal.

Essentially, range resolution is defined by the bandwidth of the received signal. A receiver bandwidth in excess of 500 MHz and typically 1 GHz is required to provide a typical resolution of between 5 and 20 cm, depending on the relative permittivity of the material.

When a number of features may be present, a signal having a larger bandwidth is required to be able to distinguish between the various targets and to show the detailed structure of a target. In this context, it is the bandwidth of the received signal that is important, rather than that of the transmitted wavelet. The material acts as a low pass filter, which modifies the transmitted spectrum in accordance with the electrical properties of the propagating medium. There are some applications of GPR, such as road layer thickness measurement, where the feature of interest is a single interface. Under such circumstances, it is possible to determine the depth sufficiently accurately by measuring the elapsed time between the leading edge of the received wavelet provided the propagation velocity is accurately known.

Although a greater depth resolution is achieved in wetter materials for a given transmitted bandwidth because of the reduced wavelength in high dielectric materials, earth materials with significant water content tend to have higher attenuation properties. This characteristic reduces the effective bandwidth, tending to balance out the change so that within certain bounds the resolution is approximately independent of loss within the propagating material.

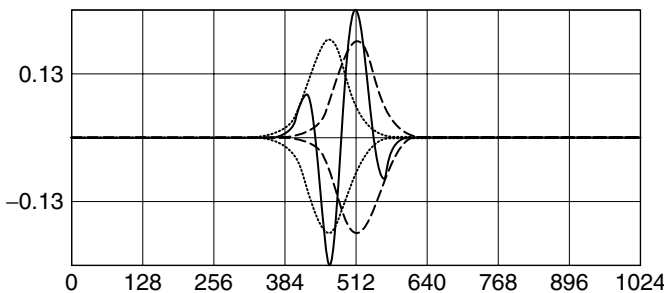


FIGURE 21.6 Two unresolved Ricker wavelets

Where interfaces are spaced more closely than one half wavelength, the reflected signal from one interface will become difficult to resolve with that from another.

It should be noted that the normal radar criteria for range resolution is less appropriate for the case of a weak target adjacent to a strong target, and there is no accepted definition of resolution for the case of unequal size targets.

**Plan Resolution.** The plan (*plan* is defined as a plane normal to the direction of propagation) resolution of a GPR system is important when localized targets are sought and when there is a need to distinguish between more than one at the same depth. Where the requirement is for location accuracy, which is primarily a topographic surveying function, the system requirement is less demanding.

The plan resolution is defined by the characteristics of the antenna and the signal processing employed. In general radar systems (apart from SAR), to achieve an acceptable plan resolution requires a high gain antenna. This necessitates a sufficiently large aperture at the lowest frequency to be transmitted. To achieve small antenna dimensions and high gain, therefore, requires the use of a high carrier frequency, which may not penetrate the material to sufficient depth. When selecting equipment for a particular application, it is necessary to compromise between plan resolution, size of antenna, the scope for signal processing, and the ability to penetrate the material. Plan resolution improves as attenuation increases, provided that there is sufficient signal to discriminate under the prevailing clutter conditions. In low attenuation media, the resolution obtained by the horizontal scanning technique is degraded, but only under these conditions do synthetic aperture techniques increase the plan resolution. Essentially the ground attenuation has the effect of placing a “window” across the SAR aperture, and the higher the attenuation the more severe the window. Hence, in high attenuation soils, SAR techniques may not provide any useful improvement to GPR systems. SAR techniques have been applied to GPR but very often in dry soils with low attenuation.

SAR techniques typically require measurements made using transmitter and receiver pairs at a number of antenna positions to generate a synthetic aperture or to focus the image. Unlike conventional radars, which generally use a single antenna, most GPR systems use separate transmit and receive antennas to provide receiver isolation. The GPR community refers to this as a bistatic mode, although actually the antenna system is closely spaced and mobile. This is different from the traditional radar community that associates the term *bistatic* with large separations.

## 21.3 MODELING

---

Models of the GPR situation range from a simple single frequency evaluation of path losses to complete 3D time-domain descriptions of the GPR and its environment. Modeling techniques include single frequency models, time-domain models, ray tracing, integral techniques, method of moments (MoM), and discrete element methods. The Finite-Difference Time-Domain (FDTD) technique has become one of the popular techniques and can be developed to run on most desktop computers with relative efficiency.

It should be noted that GPR systems often operate in intimate contact with the ground and very close to the target. Thus the antenna radiates in the near-field whereas some geophysical GPR systems operate at longer ranges (10 m to 2 km), and they

could be considered to operate in the Fresnel and even Fraunhofer (far-field) region. When the target is so close to the antenna, it interacts with the reactive fields of the antenna, and accurate models would reflect this mode of operation.

The most basic model uses the radar range equation and enables an estimate of received signal level, dynamic range, and probability of detection to be assessed. It has significant weaknesses in that most close-range GPR systems are operating in the near-field or even the reactive field of the antenna whereas the model assumes a far-field model. It is probably more relevant to the longer-range geophysical applications where the target is many tens of meters from the radar.

Many GPR receivers were originally based on sampling oscilloscope technology and the use of voltage became experimentally more useful. The most basic model for assessment of voltage signal level is derived from the radar range equation, which does have the limitations previously noted. However, it does enable a first order assessment of anticipated signal levels and an example is given in this section. The model is based on the equation for the voltage at the receiver as a function of range  $r$  and target radar cross-section  $\sigma$  and given by reference Rutledge and Muha.<sup>30</sup>

In the first model shown in Figure 21.7, the antenna is set at a height of 15 cm above the target (dielectric cylinders of 1 cm thickness, ranging in size from 0.05 m diameter to 0.5 m diameter). The target has a value of  $\epsilon_r$  of 2.2 and the soil  $\epsilon_r = 5$  and  $\tan\delta = 0.2$ . The radiated pulse has a center frequency of 1 GHz and an output pulse peak voltage of 10 volts. The radar receiver has an equivalent bandwidth of 300 MHz to 3 GHz and an equivalent receiver noise voltage of  $2.49 \cdot 10^{-5}$  volts.

The probability of detection (PD) is derived from the error function of the signal-to-noise ratio, as shown in Figure 21.8. Note that these values only relate to the receiver noise and do not include external sources of false alarms due to clutter.

The most basic model is that of the transmission line equivalent and is useful for assessing the time-domain signature of a physical situation. A conceptually simple model can be used to gain an insight into the optimum center frequency of operation and is shown in Figure 21.9.

Each layer is modeled as equivalent impedance and the transmission and reflection coefficients are calculated for each interface. The velocity of propagation and the material losses are included although not the spreading losses. The reason for this is that the received A-scan would normally have time-varying gain applied in the receiver and signal processing, and to introduce spreading loss and then compensate is an inefficient modeling exercise. In the model only the first reflection is computed, although multiple internal reflections within each layer will be generated and a full representation should include these. The parameters of the layers are given in Table 21.3.

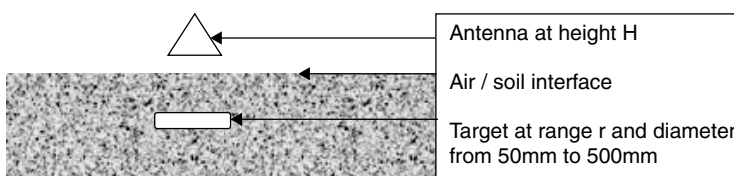


**FIGURE 21.7** Physical layout of GPR system (*Courtesy IEE*)

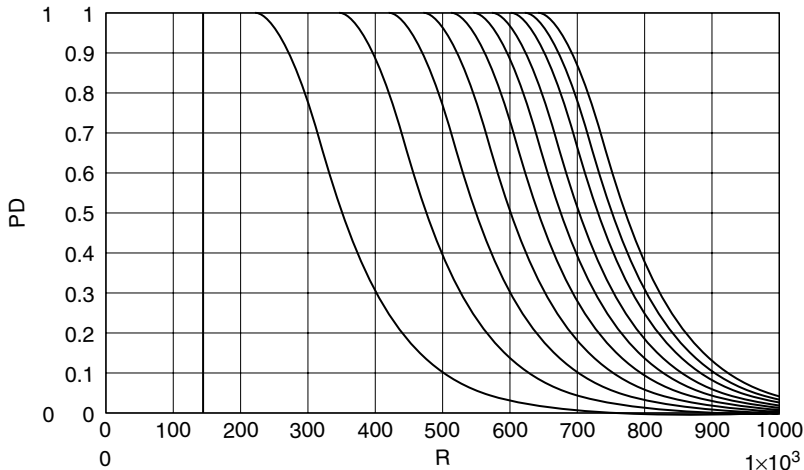


**FIGURE 21.8** Graph of probability of detection as a function of target range in millimeters and target diameter (50 mm left-hand side to 500 mm right-hand side in increments of 50 mm). Ground surface is shown as a vertical line. (*Courtesy IEE*)

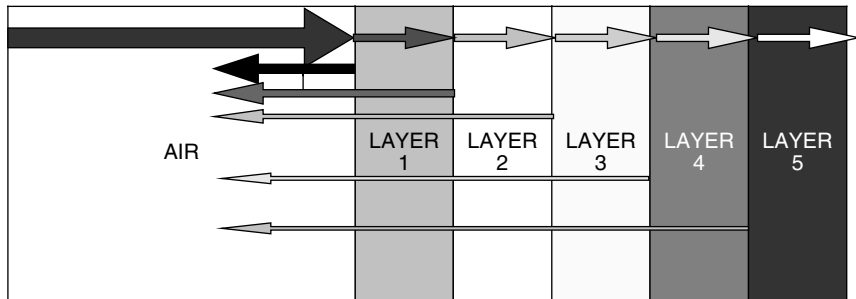


**FIGURE 21.9** Layout of transmission line model (*courtesy IEE*)

**TABLE 21.3** Layer Characteristics for Transmission Line Model

Layer	Range in Meters	Relative Dielectric Constant $\epsilon_r$	Loss Tangent	Material
0	0	1	0	Air
1	0.3	6	0.31	Lossy layer
2	0.6	1	0	Air void
3	0.85	9	0.01	Sub base
4	1	16	0.1	Wet base
5	infinite	25	0.1	Wet bedrock

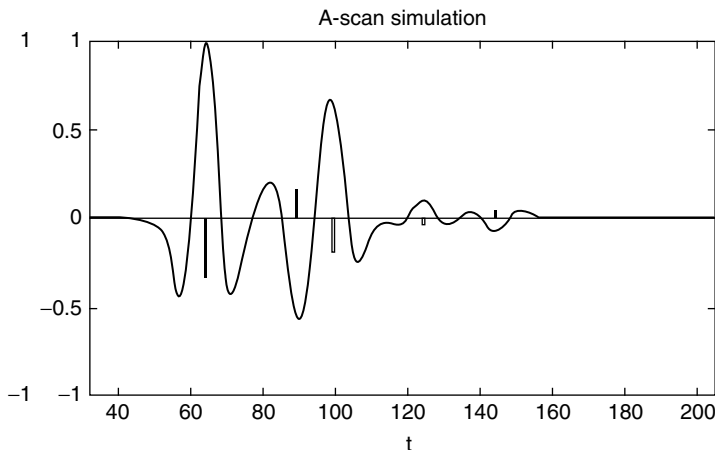


**FIGURE 21.10** Simulation of A-scan using 300 MHz center frequency (*Courtesy IEE*)

The output from the model is shown in Figure 21.10 and Figure 21.11.

Finite-Difference Time-Domain (FDTD) methods can be used to model the field propagation of a typical GPR system. The antenna used for this purpose is a resistively loaded TEM horn, as described by Martel et al.<sup>22</sup> It is 35 cm long with an aperture of 10 cm by 30 cm. The TEM horn has ultrawideband capabilities from 200 MHz to 4 GHz. It is positioned above a metallic target buried in the ground as shown in Figure 21.12. The distance between the horn aperture and the air-ground, interface is 25 cm (different from the earlier model). The modeled target is a cylinder with a radius of 3.5 cm and a height of 5 cm. It is shallowly buried at about 2.5 cm below the air-ground interface.

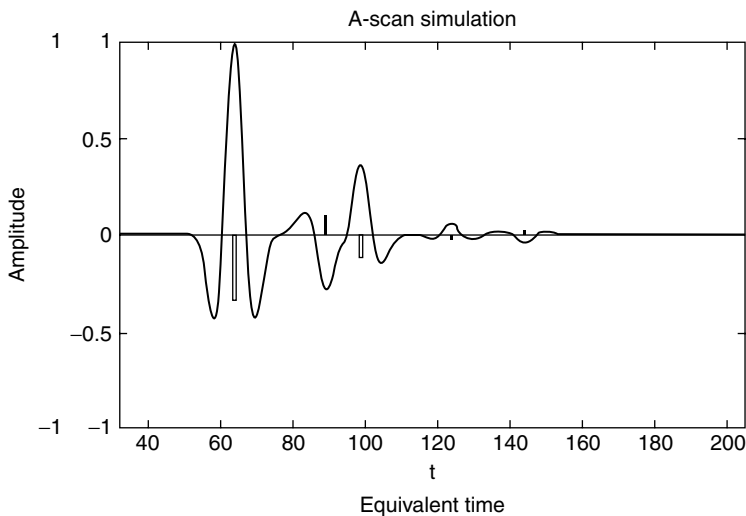


**FIGURE 21.11** Simulation of A-scan using 500 MHz center frequency (*Courtesy IEE*)

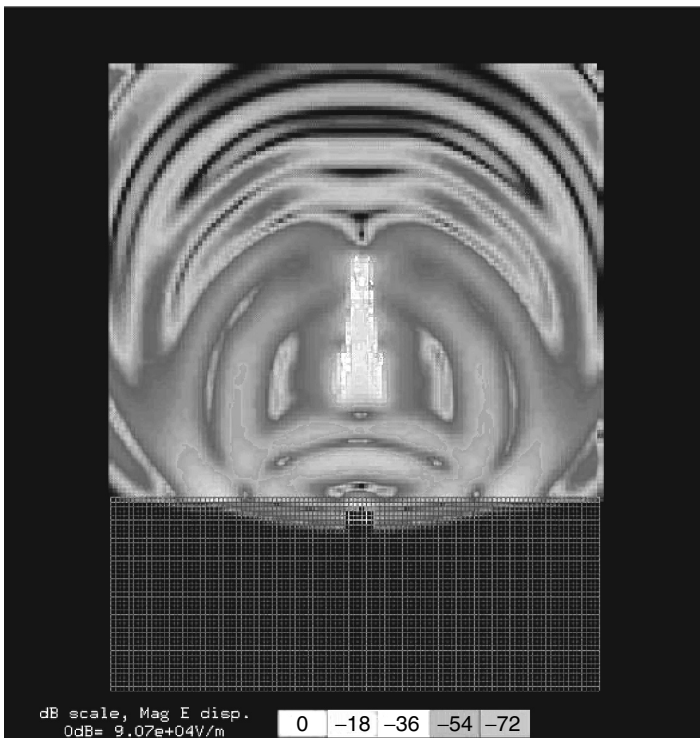


**FIGURE 21.12** Electric field plot on a vertical cut plane after the main ground reflection (*Courtesy IEE*)

The ground is modeled as a uniform lossy material with a relative permittivity of 13 and a conductivity of 0.005 S/m (Siemens/meter). The air-ground interface is assumed to be perfectly flat.

From the field plot, one can recognize the antenna structure and the strong field region on and inside the horn plate. The buried object is also visible. The main reflection caused by the air-ground interface can clearly be seen coming back toward the antenna system. In addition, a weaker reflection coming from the buried object is starting to form and follows the air-ground interface reflection in time. This is a typical time-domain characteristic of standoff GPR system. Moreover, other physical phenomena can be observed such as the free space path loss and the reduction in velocity of propagation in the ground.

It should be noted that the process of physically scanning the antenna system over the target creates a hyperbolic image of the target, as shown in Figure 21.13. For the two-dimensional case ( $x$  = position on surface and  $z$  = depth to the target) of a material with known constant velocity, the measured time to the point reflector is given by  $t$  and then the distance to the point reflector is given by  $z = vt/2$ . At any position along the  $x$ -axis the distance  $z$  is also given by

$$z_i = \sqrt{(x_i - x_0)^2 + z_0^2} \quad (21.11)$$

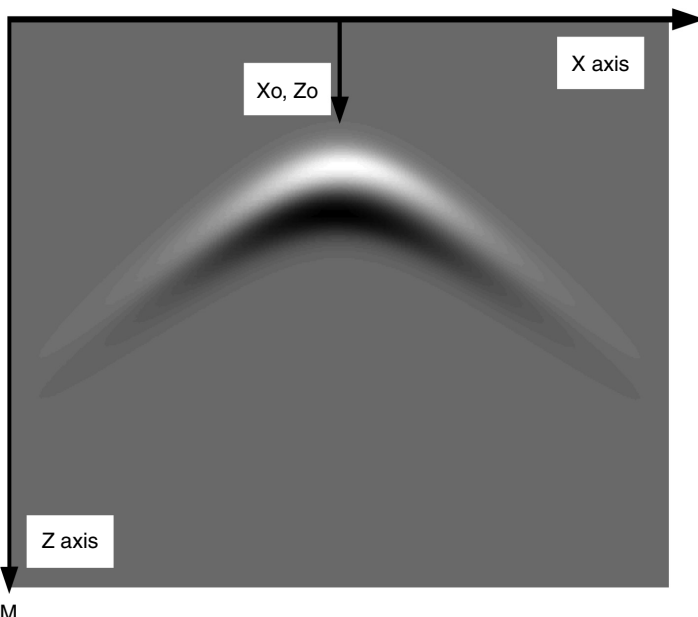


**FIGURE 21.13** Typical hyperbolic image of GPR data from a reflector of circular cross section (*Courtesy IEE*)

This equation shows that the measured wavefront appears as a hyperbolic image or a curve of maximum convexity. Migration technique may be used to move or migrate a segment of an A-scan time sample to the apex of a curve of maximum convexity. The hyperbolic curve needs to be well-separated from other features and a good signal-to-noise ratio is needed for this technique to work well.

## 21.4 PROPERTIES OF MATERIALS

---

The determination of the dielectric properties of earth materials remains largely experimental. Rocks, soils, and concrete are complex materials composed of many different minerals in widely varying proportions, and their dielectric parameters may differ greatly even within materials that are nominally similar. Most earth materials contain moisture, usually with some measure of salinity. Since the relative permittivity of water is in the order of 80, even small amounts of moisture cause a significant increase of the relative permittivity of the material. A large number of workers have investigated the relationships between the physical, chemical, and mechanical properties of materials and their electrical and, in particular, microwave properties. In general, they have sought to develop suitable models to link the properties of the material to its electromagnetic parameters. Such models provide a basis for understanding the behavior of electromagnetic waves within these media. The real and imaginary dielectric losses

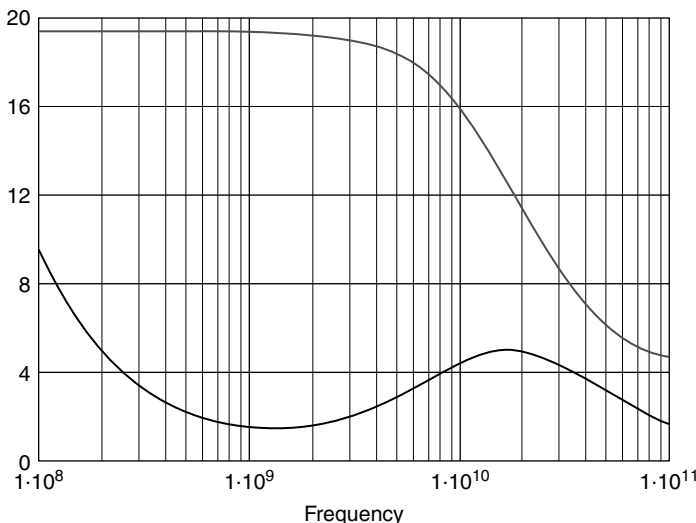


**FIGURE 21.14** Dielectric properties  $\epsilon'$  (upper) and  $\epsilon''$  (lower) of lossy soil as a function of frequency (*Courtesy IEE*)

as a function of frequency can be plotted over a wide frequency range and a typical result is shown in Figure 21.14.

Information on the geological properties of earth soils can be found in the Digital Soil Map of the World and Derived Soil Properties CD, published by the Food and Agriculture Organization of the United Nations. This enables the ten map sheets of the world to be classified in terms of parameters such as pH (concentration of hydrogen ions), organic carbon content, C/N (carbon-to-nitrogen) ratio, clay mineralogy, soil depth, soil moisture capacity, and soil drainage class. Such information is useful in assessing the potential of RF techniques and particularly GPR for particular geographic regions.

There are two benefits to understanding soil properties in relation to GPR. The first is to understand the applicability of GPR to particular soils and hence the possibility of using GPR to detect buried targets such as pipe, cables, landmines, etc. The second is to use GPR to characterize soils and soil properties.

GPR can provide a detailed map of the subsurface, which when combined with traditional soil survey methods can provide information on the type of soil, its extent laterally and in depth, the water table, the layering and features of the soil, and hence its local geology and history.

GPR has been used in the U.S. by the Department of Agriculture-Natural Resources Conservation Service (USDA-NRCS) as a quality control tool for soil mapping and investigations. The use of GPR in soil survey activities has provided information about soil resources that would have been unobtainable by other means or would have been uneconomical to obtain. An example of the results of this work is shown in Figure 21.15.

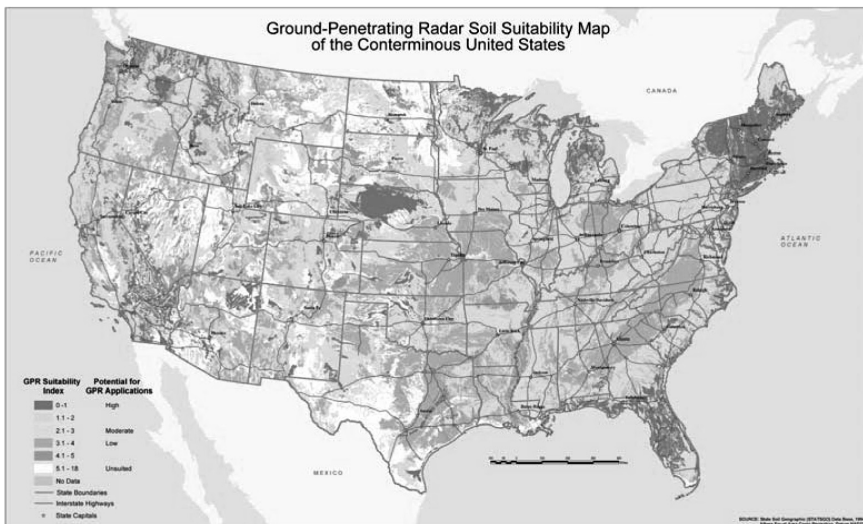


**FIGURE 21.15** GPR Soil Suitability Map of the Continental (Conterminous) United States (*Courtesy of USDA-NRCS*)

## 21.5 GPR SYSTEMS

The choice of system design is to a large extent governed by the type of target, the resolution required, and the anticipated ground attenuation and clutter. The depth range of the radar system is likely to be primarily defined by the soil attenuation, once a particular range of frequencies has been chosen. However, it can be shown that considerable variations (10–30 dB) in the sensitivity of competing system designs actually translate to relatively small changes in depth performance in lossy soils.

The selection of a suitable waveform for transmission, at least in terms of resolution, can be considered a function of the duration of the complex envelope of the signal. The output from most ultrawideband radar systems can be compared in terms of a time-domain representation of the waveform. Almost all types of radar can be assessed not just by their signal-to-noise and signal-to-clutter ratios but also by comparing their inherent range sensitivity. Such a procedure reveals the characteristics that control the radar performance. The design of a GPR system is defined by the modulation technique, and time domain, frequency domain, and pseudo-random-coded domain radar designs are most likely to be encountered. Frequency domain radars may use either stepped frequency or continuously swept frequency modulation. They transmit, on a repetitive basis, a nominally constant amplitude signal whose frequency increases in a linear progression from the lowest to the highest value.

Recovery of the receiver signal from noise may be achieved by either conventional bandpass filters or by the matched filter or Wiener filter.

The fundamental operation of a matched filter is correlation. The amplitude of each point in the output signal is a measure of how well the filter kernel matches the corresponding section of the input signal. The output of a matched filter does not necessarily look like the signal being detected, but if a matched filter is used, the shape of the target signal must already be known. The matched filter is optimal in the sense

that the peak signal output to mean noise ratio is greater than can be achieved with any other linear filter. This is not always the best filter to use for time-domain waveforms where the fidelity of the output may be a requirement.

The Wiener filter separates signals based on their frequency spectra. The gain of the Wiener filter at each frequency is determined by the relative amount of signal and noise at that frequency: The Wiener and matched filter must be carried out by *convolution*, making them extremely slow to execute.

The matched filter radar receiver provides an optimum linear processing of radar in the presence of noise. The radar signal is processed by a filter that cross-correlates the received waveform with a suitably time-delayed version of the transmitted waveform. The output results in an output in which the amplitude of the latter and its position in delay time is related to the target radar characteristic. This type of receiver is widely used to process chirp, step frequency, and pseudo-random-coded waveforms, and the design of such waveforms is extensively described in the literature.

Many commercial time-domain radar systems use a sampling receiver to down-convert the radar signals from the nanosecond time frame to a millisecond time frame that is easier to post process. However, a real disadvantage of the sampling receiver is its limited dynamic range due to the sampling diodes and inherently high noise level due to its wide bandwidth. Details of typical sampling receivers, which are essentially the same as sampling oscilloscopes, can be found in the literature, and once issues of sampling linearity in time are addressed, the generic design has formed the basis for the majority of commercial GPR systems.

A key parameter for most GPR systems is the mean power. The time-domain radar transmits, on a repetitive basis, a short duration impulse. Consequently, its peak power is significantly greater than its mean power. This is not the case with stepped frequency whose radiated power per spectral line is higher than the time-domain radar that gives an advantage in terms of transmitter peak signal capability compared with the impulse GPR.

## 21.6 MODULATION TECHNIQUES

---

There are three main modulation techniques: time domain, frequency domain, and pseudo-random-coded radar. GPR systems that transmit an impulse and receive the reflected signal from the target using a sampling receiver can be considered to operate in the time domain. GPR systems that transmit individual frequencies in a sequential manner and receive the reflected signal from the target using a frequency conversion receiver can be considered to operate in the frequency domain. The latter systems often reconstruct the downconverted frequencies to recover a time-domain replica of the signal.

All GPRs may have to detect signals from a target that may be  $-50$  to  $-100$  dB lower than the radiated signal at ranges in the order of a meter (6.6 ns in free space). In addition, the received signal will contain temporal scattering information on the target that can be exploited.

The temporal fidelity of received signal needs to be preserved and thus designers of GPR have to ensure that the receiver is not saturated by the transmitted signal, the antennas do not cause time sidelobes, and the receiver does not distort the received signal.

**Time Domain.** Most commercially available GPR systems use short pulses or impulses such as the Ricker wavelet, as shown previously in Figure 21.5. The high-speed sequential sampling approach used to acquire RF waveforms produces a low

SNR because the spectrum of the sampling pulse is a poor match for that of the received pulse. In general, the dynamic range of the sampling receiver is typically 60 dB, without range (time) varying gain. The effect of the range varying gain is to enable the lower amplitude signals from targets at a greater range to be amplified so as to be above the minimum sampling threshold signal level. This is equivalent to a linear receiver with a 90 dB or more dynamic range. Signal averaging or integration of the samples can increase the effective sensitivity by the amount of averaging and this can be typically 10 to 30 dB. The ratio of the peak transmitted signal to the mean receiver noise level can be up to 150 dB.

The antennas that can be used with time-domain GPR are limited to linear phase designs such as resistively loaded dipoles, TEM horns, or Impulse Radiating Antennas (IRAs). It should be noted that ultrawideband antennas fall into two classes, those that radiate a reasonably short impulse with low time sidelobes and fundamentally possess a linear phase-frequency characteristic. The alternative class of antennas, such as log periodics, have wideband frequency characteristics but nonlinear phase-frequency characteristics. Essentially, the latter class will cause the different frequency components of an impulse to be radiated at different times, hence dispersing the impulse. If such antennas are used with time-domain radar, the dispersive properties of the antenna used must be compensated by suitable post-processing filtering.

The time-domain radar system transmits a sequence of pulses, typically of amplitudes within the range between 20 V to 200 V and pulse widths within the range between 200 ps to 50 ns at a pulse repetition interval of between several hundred microseconds to one microsecond, depending on the system design. The impulse generator is generally based on the technique of rapid discharge of the stored energy in a short transmission line. The most common method of achieving this is by means of a transistor operated in avalanche breakdown mode used as the fast switch and a very short length of transmission line. It is quite feasible to generate pulses of several hundred kV albeit at long repetition intervals. The output from the receive antenna is applied to a flash A/D converter or a sequential sampling receiver. The latter normally consists of an ultrahigh speed sample and hold circuit. The control signal to the sample and hold circuit, which determines the instant of sample time, is sequentially incremented at each pulse repetition interval. For example, a sampling increment of  $t = 100$  ps is added to the previous pulse repetition sampling interval to enable sampling of the received signal at regular intervals as indicated in Figure 21.16.

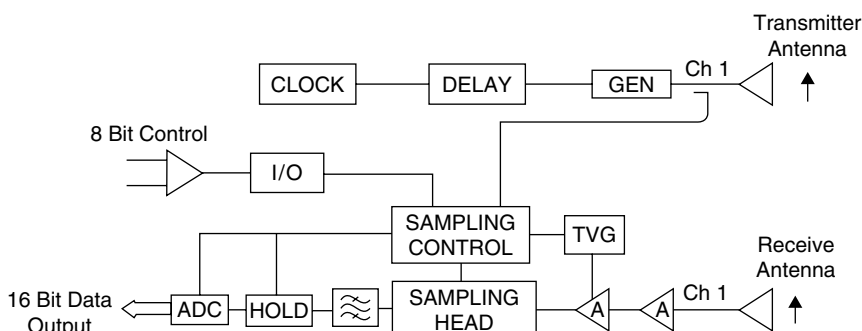


**FIGURE 21.16** Typical sampling receiver used for time-domain GPR systems

The principle of the sampling receiver is, therefore, a downconversion of the radio frequency signal in the nanosecond time region to an equivalent version in the micro- or millisecond time region. The incrementation of the sampling interval is terminated at a stage when, for example, 256, 512, or 1024 sequential samples have been gathered. The process is then repeated. There are several methods of averaging or “stacking” the data; either a complete set of samples can be gathered and stored and further sets added to the stored data set, or alternatively, the sampling interval is held constant for a predetermined time to accumulate and average a given number of individual samples. The first method needs a digital store but has the advantage that each waveform set suffers little distortion if the radar is moving over the ground.

The second method does not need a digital store and a simple low-pass analogue filter can be used. However, depending on the number of samples that have been averaged, the overall waveform set can result in being “smeared” spatially if the radar is moving at any speed. The stability of the timing increment is very important and generally this should be 10% of the sampling increment; however, practically a stability in the order of 10 ps to 50 ps is achieved. The effect of timing instability is to cause a distortion, which is related to the rate of change of the RF waveform. Evidently, where the RF waveform is changing rapidly, jitter in the sampling circuits results in a very noisy reconstructed waveform. Where the rate of change of signal is slow, jitter is less noticeable. Normally, control of the sampling converter is derived from a sample of the output from the pulse generator to ensure that variations in the timing of the latter are compensated automatically. The key elements of this type of radar system are the impulse generator, the timing control circuits, the sampling detector, and the peak hold and analogue to digital converter.

**Frequency Domain Radar.** The main potential advantages of the frequency domain radar are the wider dynamic range, lower noise figure, and higher mean powers that can be radiated. There are two main types of frequency domain radar, Frequency Modulated Carrier Wave (FMCW) and Stepped Frequency Carrier Wave (SFCW). FMCW radar transmits a continuously changing frequency over a chosen frequency range on a repetitive basis. The received signal is mixed with a sample of the transmitted waveform and results in a difference frequency, which, although fundamentally related to the phase of the received signal, is a measure of its time delay and hence range of the target. The difference frequency or intermediate frequency (IF) must be derived from an I/Q mixer pair if the information equivalent to a time-domain representation is required (i.e., to reconstitute an impulse), as a single-ended mixer only provides the modulus of the time-domain waveform. The basic FMCW radar system is particularly sensitive to certain parameters. In particular, it requires a high degree of linearity of frequency sweep with time to avoid spectral widening of the IF and hence degradation of system resolution. Dennis and Gibbs<sup>23</sup> made an assessment of the sensitivity of time sidelobe level to linearity and showed the ratio of sidelobe to peak level was dependent on the sweep linearity. Practically, the effect of a nonlinearity of a few percent is to cause significant time sidelobes, as this needs to be compensated in the transmitter modulator design.

The SFCW radar transmits a series of incremental frequencies and stores the received IF signal to then carry out a Fourier transform reconstruction of the time-domain equivalent waveform. The SFCW has found many applications in GPR because the requirements on scan rate are relatively modest. The impact of mobile communications technology has had a significant impact on reducing the cost of radar components for this design. Two forms of the synthesized radar can be considered.

The first and simplest system is stepped frequency continuous wave radar. The second form is more complex in that each individual frequency is appropriately weighted in amplitude and phase prior to transmission. Normally, the radar is calibrated both to establish a reference plane for measurement as well as to reduce the effect of variations in the frequency characteristics of components and antennas.

A much wider class of antenna is available for use by the designer of frequency domain radars. The noise floor of the receiver is much lower than the time-domain equivalent, simply by virtue of its lower bandwidth and hence lower thermal noise. Typically, a sensitivity of  $-120$  dBm is found and a system peak transmitted signal to mean receiver noise range of  $180$  dB is feasible. It should be noted that the IF bandwidth of the receiver in FMCW and SFCW systems can be made relatively small whereas the sampling receiver in the time-domain receiver has a bandwidth of many GHz and hence a poor noise performance.

The main potential advantage of a stepped frequency or FMCW GPR is its ability to adjust the range of frequencies of operation to suit the material and targets and electromagnetic environment under investigation if the antenna has an adequate passband of frequencies. It can radiate a higher mean power level per spectral line than the time-domain radar, and its ability to integrate the received signal level improves the system sensitivity. The calibration of the radar does, of course, depend on stable system characteristics and antenna parameters that are invariant with the spacing of the front surface and the antenna. Although on first consideration, frequency domain radars should offer a superior sensitivity to time-domain radars, because of their lower IF receiver bandwidth and hence thermal noise, both the type of receiver and the range sidelobes of the radiated spectrum may result in an equivalent or worse sensitivity in terms of range resolution as discussed above.

**Pseudo-random-coded Radar.** Work has been carried out on pseudo-random-coded modulation techniques for GPR. The main advantage of this method is that the energy transmitted is spread more evenly over the spectrum than with any other modulation method and hence the likelihood of interference to other users of the spectrum is minimized. In addition, the chances of other users of, say, mobile phones interfering with the GPR operator are also reduced. The mean power is the lowest of any of the modulation schemes and this is helpful in meeting regulatory requirements.

The transmitted signal has noise-like characteristics and the received signal is cross-correlated with a sample of the transmitted signal. The range of the target is given by the time position of the cross-correlated signal and the amplitude by the peak of the cross-correlated signal. Control of the cross-correlation sidelobes is vital to achieve good range resolution and the sidelobes are affected by the antenna and system characteristics as well as the duration and randomness of the transmitted waveform. Further information is given by Narayanan<sup>24</sup> and Sachs et al.<sup>25,26</sup>

## 21.7 ANTENNAS

---

In the ultrawideband case, the radar antennas are considered in terms of their transfer function rather than their gains or effective apertures. In many cases, a separate transmit and receive antenna is used; hence their transfer functions may not be identical. The type of antenna that is used with ultrawideband radar has an important role in defining the performance of the radar.

Element antennas are characterized by linear polarization, low directivity, and relatively limited bandwidth, unless either end-loading or distributed-loading techniques are employed in which case bandwidth is increased at the expense of radiation efficiency. An elemental antenna is a dipole in contrast to aperture antennas such as horns. A normal short dipole antenna fed with a very short current impulse will radiate from the feed points and the end of the element because of the latter's discontinuity as far as current flow is concerned. The current impulse will be reflected from the end of the dipole and travel up and down the dipole causing a series of impulses of radiation. This extends the time signature of the radiated waveform and degrades the range resolution of the system. This effect is shown in Figure 21.17 where the radiation pattern is shown at a time several pulse durations after application. The outer perimeter represents the energy radiated at time zero followed at intervals by the radiation from the feed points and the end of the element.

As it is required to radiate only a very short impulse, it is important to eliminate the reflection discontinuities from the feed points and ends of the antenna either by end loading or by reducing the amplitude of the charge and current reaching the ends. The latter can be achieved either by resistively coating the antenna or by constructing the antenna from a material such as Nichrome, which has a defined loss per unit area. In this case, the antenna radiates in a completely different way as the applied charge becomes spread over the entire element length, and hence, the centers of radiation are distributed along the length of the antenna. Typical radiated field patterns for a resistively loaded dipole are shown in Figure 21.18. However, the reduction in impulse duration is achieved at the expense of efficiency and loaded antennas may have efficiencies as low as 10%.

The types of antennas that are useful to the designer of ultrawideband radar fall into two groups: dispersive antennas and nondispersive antennas. Dispersive antennas have a nonlinear phase/frequency response whereas nondispersive antennas have a substantially linear phase/frequency response. Examples of dispersive antennas that have been used in ultrawideband radar are the exponential spiral, the Archimedean

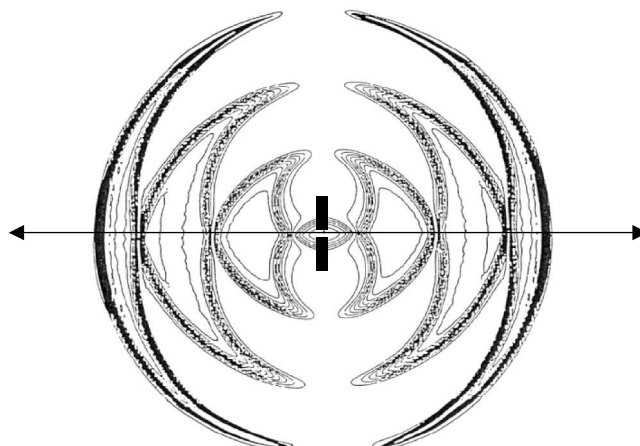


**FIGURE 21.17** Radiated field pattern from a conducting dipole element due to an applied impulse (*Courtesy IEE*)

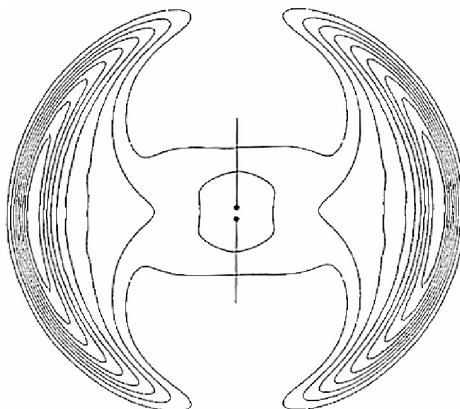


**FIGURE 21.18** Radiated field pattern from a resistively loaded dipole element due to an applied impulse  
(Courtesy IEE)

spiral, the logarithmic planar antenna, the Vivaldi antenna, slot antennas, and the exponential horn. The impulse response of this class of antennas generally results in a waveform whose time frequency response is extended (and is similar to a chirp, albeit with an inconstant amplitude) if the input is an impulse.

Examples of nondispersive antennas are the TEM horn, the bicone; the bow tie; the resistive, lumped element-loaded antenna, and the continuously, resistively loaded antenna. The input voltage driving function to the terminals of the antenna in impulse radar is typically a narrow gaussian pulse of 200 ps, and this requires the impulse response of the antenna to be extremely short. The main reason for requiring the impulse response to be short is that it is important that the antenna does not distort the input function and generate time sidelobes. These time sidelobes would obscure targets that are close in range to the target of interest; in other words, the resolution of the radar can become degraded if the impulse response of the antenna is significantly extended.

However, in principle, all antennas are dispersive to some extent but nondispersive antennas do not need correction in the signal processing, which reduces the overall complexity of the radar processing. The very short range operation of many GPR systems enables operation of antennas in a way that does not conform to traditional analytic models of antenna gain and aperture.

Horn antennas have found most use with FMCW ultrawideband radars where the generally higher frequency of operation and relaxation of the requirement for linear phase response permit the consideration of this class of antenna. FMCW ultrawideband radars have used an offset paraboloid fed by a ridged horn. This arrangement was designed to focus the radiation into the ground at a slant angle to reduce the level of the reflection from the ground. Care needs to be taken in such arrangements to minimize the effect of back and sidelobes from the feed antenna, which can easily generate reflection from the ground surface.

One method of radiating circular polarization is to use an equi-angular spiral antenna. The dispersive nature of this type of antenna causes an increase in the duration of the transmitted waveforms, and the radiated pulse takes the form of a “chirp”

in which high frequencies are radiated first, followed by the low frequencies. A “spiking” filter, which may take the form of a conventional matched filter, however, may compensate for this effect, or a more sophisticated filter such as Wiener filter, which recovers the original shape of the waveform, applied to the antenna.

It is important to appreciate the effect of the material in close proximity to the antenna. In general this material, which in most cases will be soil or rocks or indeed ice, can be regarded as a lossy dielectric and by its consequent loading effect can play a significant role in determining the low frequency performance of the antenna and hence GPR. The behavior of the antenna is intimately linked with the material and, in the case of borehole radars, the antenna actually radiates within a lossy dielectric, whereas in the case of the GPR working above the surface, the antenna will radiate from air into a very small section of air and then into a lossy half space formed by the material. The behavior of antennas both within lossy dielectrics and over lossy dielectrics is well reported. The propagation of electromagnetic pulses in a homogeneous conducting earth has been modeled by Wait<sup>27</sup> and King,<sup>28</sup> and the dispersion of rectangular source pulses suggests that the time-domain characteristics of the received pulse could be used as an indication of distance.

The interaction between the antenna and the lossy dielectric half space is also significant as this may cause modification of the antenna radiation characteristics both spatially and temporally and should also be taken into account in the system design. In the case of an antenna placed on an interface, the two most important parameters are the current distribution and the radiation pattern. At the interface, currents on the antenna propagate at a velocity, which is intermediate between that in free space and that in the dielectric. In general, the velocity is retarded by the  $\sqrt{(\epsilon_r + 1)/2}$ . The net result is that evanescent waves are excited in air, whereas in the dielectric the energy is concentrated and preferentially induced by a factor of  $n^3:1$ .

The respective calculated far-field power density patterns, in both air and dielectric, are given by Rutledge<sup>29</sup> (see Table 21.4), and these are plotted for a relative dielectric constant of 9 in Figure 21.19 and Figure 21.20. For comparison, the far-field pattern of a dipole radiating into free space is shown in Figure 21.21.

The above expressions in Table 21.4 assume that the current source contacts the dielectric, whereas a more general condition is when the antenna is just above the dielectric. A significant practical problem for many applications is the need to maintain sufficient spacing to avoid mechanical damage to the antenna. It can, therefore, be appreciated that the effect of changes in distance between the antenna and half space is to cause significant variation in the resultant radiation patterns in the dielectric.

A particularly useful antenna capable of supporting a forward traveling TEM wave is the TEM horn. In general, such antennas consist of a pair of conductors either

**TABLE 21.4** Power Density Patterns in Air and Dielectric

	Power	Power
Plane H	Radiation pattern in dielectric x direction	Radiation pattern in dielectric y direction
E	$\alpha \left( \frac{\cos \theta_a}{\cos \theta_a + \eta \cos \theta_d} \right)^2$	$\alpha \eta \left( \frac{\eta \cos \theta_d}{\cos \theta_a + \eta \cos \theta_d} \right)^2$
	$\alpha \left( \frac{\cos \theta_a \cos \theta_d}{\eta \cos \theta_a + \cos \theta_d} \right)^2$	$\alpha \eta \left( \frac{\eta \cos \theta_a \cos \theta_d}{\eta \cos \theta_a + \cos \theta_d} \right)^2$

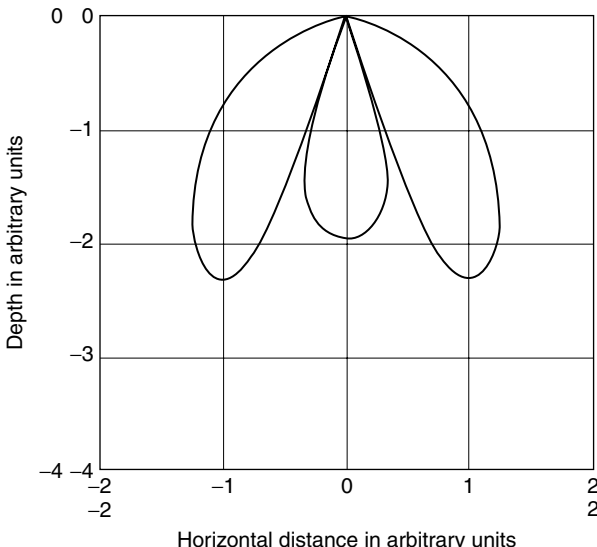


**FIGURE 21.19** E-plane plot of far-field power density of a current element radiating into a lossless material of dielectric constant of 9

flat, cylindrical, or conical in cross section, forming a V structure in which radiation propagates along the axis of the V structure. Although resistive termination is used, this type of antenna has a directivity on the order of 10–15 dB depending on size; hence, useful gain can still be obtained even with a terminating loss on the order of

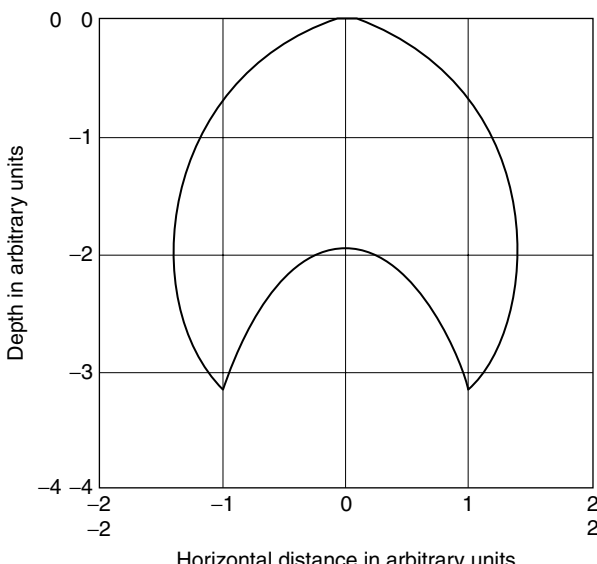


**FIGURE 21.20** H-plane plot of far-field power density of a current element radiating into a lossless material of dielectric constant of 9

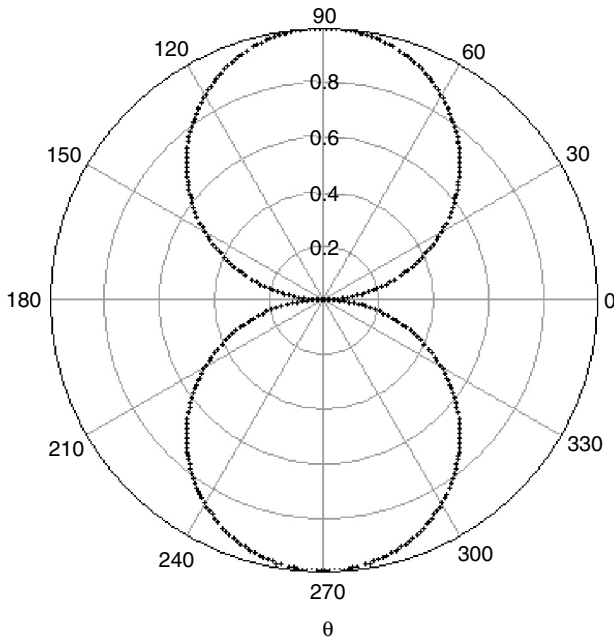


**FIGURE 21.21** H-plane plot of far-field power density of a current element radiating into free space

3 dB to 5 dB. A further development of the TEM horn is given by Martel<sup>21</sup> in which the antenna is composed of a set of spread “fingers” forming the shape of a horn as shown in Figure 21.22. Each finger is a wire with a diameter of 1 mm and is resistively loaded at different locations along the length of the antenna. The feed component for the antenna is comprised of a 50 Ohm coax, feeding a tapered parallel plate waveguide with a width of 30 mm and a height of 7 mm. A taper along the width of the top parallel plate is used as a transition to transform a 50 Ohm unbalanced line into a 50 ohm balanced line.

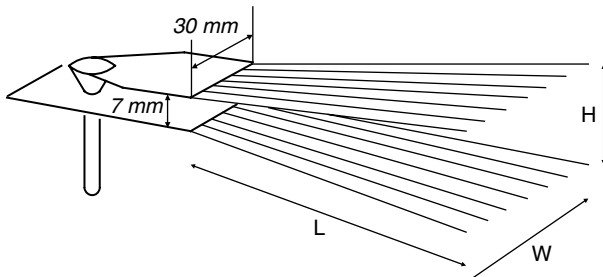


**FIGURE 21.22** Antenna and feed geometry of loaded TEM horn,  $L = 30$  cm (Courtesy IEE)

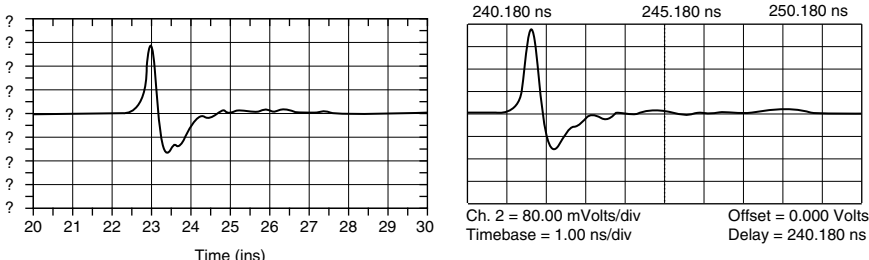


**FIGURE 21.23** Predicted and actual pulse responses of loaded TEM horn antenna (*Courtesy IEE*)

The predicted and actual time-domain pulse of the optimum design is shown in Figure 21.23. The shape of the time-domain antenna response is similar to a second derivative gaussian signal. It can be seen that most of the internal reflections have been suppressed. The rate of decrease for the unwanted ringing is better than 9 dB/ns. The VSWR was better than 2:1 from 100 MHz to 5.8 GHz.

There are many configurations of antenna that can be used; crossed dipoles and parallel dipoles are the most popular. The main reason for the use of two antennas is that TR switches that are fast enough for GPR are not yet available.

## 21.8 SIGNAL AND IMAGE PROCESSING

---

The three basic permutations of GPR data presentation are shown in Figure 21.24. The most basic GPR data record is an A-scan. An A-scan provides amplitude-time record of a single measurement over a target. Only amplitude-range information is plotted. GPR is generally used in such a way as to generate a sequence of A-scans related to the survey position on the ground surface. This sequence can be termed a B-scan and an example is shown in Figure 21.24. This effectively represents one axis (z) depth and the orthogonal axis (x or y) linear position. The amplitude of the signal may be shown as a series of overlapping signals or, alternatively, a “wiggle plot” (borrowed from seismic terminology) or a grayscale-coded intensity plot or a pseudo-color image. In the modeled example shown, the hyperbolic spreading of the target spatial response can be seen. As shown in Figure 21.24, a C-scan consists of a plan view (x, y plane over a defined range of depth z). Note that these terms are not the same as used in conventional radar display.

The received time waveform can be described as the convolution of a number of time functions each representing the impulse response of some component of the radar system in addition to noise contributions from various sources. Note that two antennas are used: one transmits and one receives.

$$s_r(t) = s_s(t) \otimes s_{\text{af}}(t) \otimes s_c(t) \otimes s_{\text{gf}}(t) \otimes s_t(t) \otimes s_{\text{gr}}(t) \oplus s_{\text{ar}}(t) + n(t) \quad (21.12)$$

where

$s_s(t)$  = signal applied to the antenna

$s_{\text{ad}}(t)$  = antenna impulse response

$s_c(t)$  = antenna cross coupling response

- $s_{gd}(t)$  = ground impulse response  
 $s_t(t)$  = impulse response of target  
 $n(t)$  = noise

( $d$  denotes direction— $f$  being forward and  $r$  reverse direction)

Each contribution has its own particular characteristics that need to be considered carefully before application of a particular processing scheme. Ideally the signal applied to the antenna should be a Dirac function but practically it is more like a skewed gaussian impulse of defined time duration. Most antennas used in surface penetrating applications have a limited low frequency response and tend to act as high-pass filters, effectively differentiating the applied impulse and hence creating a time-limited function. In most cases, near identical antenna are used, and if these are spaced sufficiently far from the ground surface, then  $s_{af}(t) = s_{ar}(t)$ . In the case of antennas operated in close proximity to the ground, then both  $s_{af}(t)$  and  $s_{ar}(t)$  are variant with

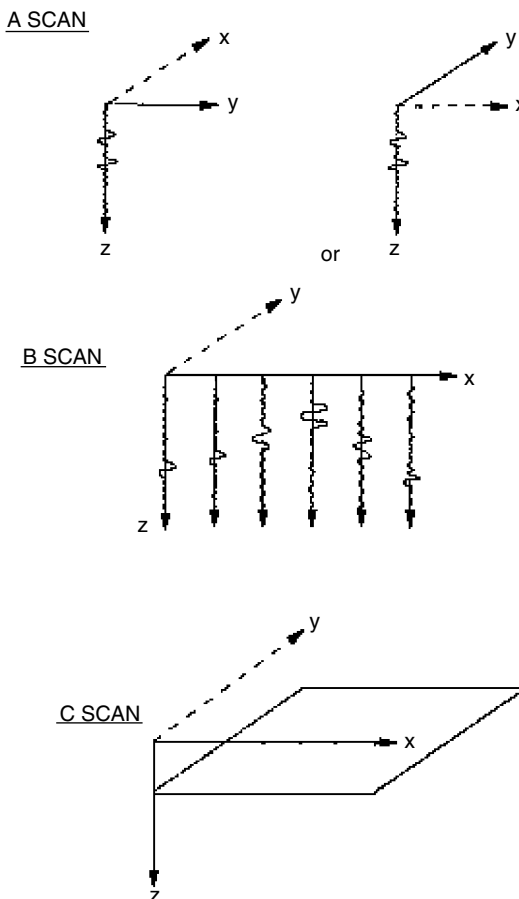


FIGURE 21.24 Coordinate system for scan description  
 (Courtesy IEE)

changes in the ground surface electrical parameters. Essentially the impedance of the antenna is changed by its proximity to the ground; hence it cannot be considered to have a stable impulse response.

Any processing scheme that relies on invariant antenna parameters should take into account the mode of operation of the antennas and the degree of stability that is practically realizable. The antenna cross coupling response  $s_c(t)$  is composed of a fixed contribution  $s'_c(t)$  due to antenna cross coupling in air and a variable contribution  $s''_c(t)$  due to the effect of the ground or nearby objects. Hence  $s_c(t) = s'_c(t) + s''_c(t)$ . It has been found possible to reduce the amplitude of  $s_c(t)$  to very low levels, in the case of crossed dipole antennas to below  $-70$  dB simply by attention to the precision of construction, and in the case of parallel dipole antennas to below  $-60$  dB by the interposing between the antennas of suitable absorbing material. However,  $s''_c(t)$  can be significantly larger and degrades the overall value of  $s_c(t)$  to  $-40$  dB. The value of  $s_a(t)$  is determined by any local inhomogeneities in the soil or by any covering material whether of mineral or vegetable origin. There is unfortunately little that can be done to predict variations in  $s''_c(t)$ , and it is not amenable to treatment by many processing algorithms. The variation in  $s''_c(t)$  is much greater with the crossed dipole antenna than the parallel dipole. The ground impulse response  $s_g(t)$  can be determined from its attenuation and dielectric constant across the frequency range of interest.

The target impulse response can be composed of the convolution of the wanted target response, together with many other reflectors, which may not be wanted by the user but which are valid reflecting targets as far as electromagnetic waves are concerned. The time separation of the targets is related to their physical spacing as well as the velocity of propagation, which can vary depending on the material properties.

Where the targets are well separated in range, it is relatively straightforward to separate the radar reflections, but this becomes progressively more difficult as targets become closer together, as instead of separable time-domain signatures the reflections will merge together.

As the antennas generally used for GPR have poor directivity, the pattern of the reflected waveform in the B-scan represented the spatial convolution of the antenna pattern with the target. The reader is referred to Figure 21.13, shown previously, which illustrates this effect. This spatial pattern does not represent an image of the object of interest and much effort has been made to develop methods to reconstruct the target image from GPR data.

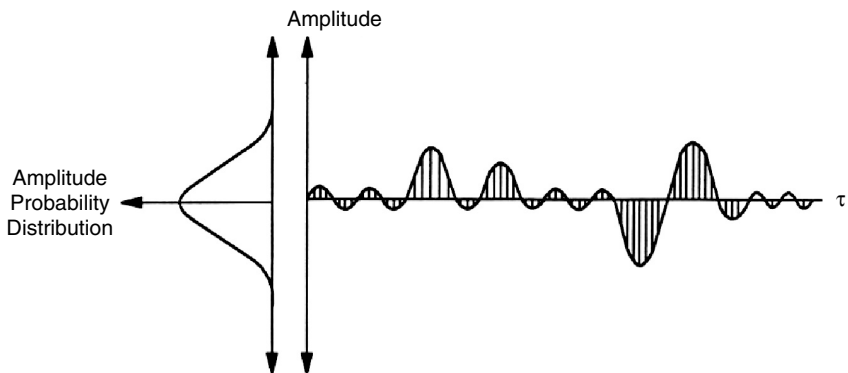


**FIGURE 21.25** Envelope of A-scan sample time series (Courtesy IEE)

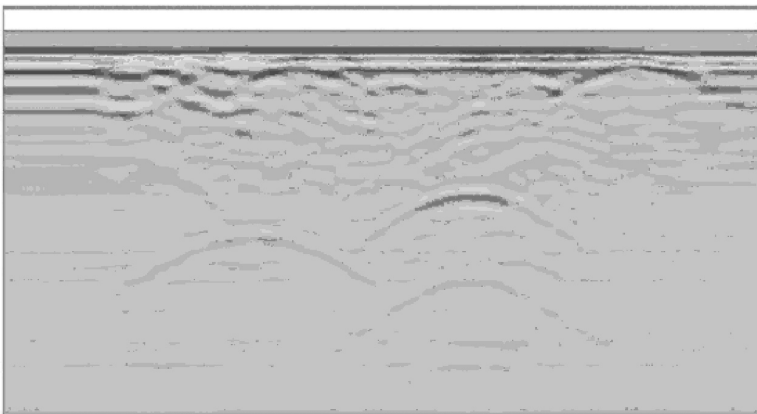


**FIGURE 21.26** B-scan unprocessed data (*Courtesy IEE*)

Deconvolving the image using any of the following processes can do this; synthetic aperture processing, conjugate gradient methods, and reverse time migration are extensively reported in the literature. Many of these techniques work well on isolated targets such as pipes, which have well-defined geometrical boundaries. The situation is more difficult with stratified layers and, of course, anisotropic materials.

When a reconstructed image of the buried object is created, whether as a B-scan or C-scan (area at a particular range of depths), it is necessary to interpret the radar image as being generated by a physical structure. This is not always easy in the case of a cluttered image, and a great deal still depends on the field experience of the operator. Examples of unprocessed B-scan data and the same corrected for spreading loss and attenuation are shown in Figure 21.26 and Figure 21.27.

Although a C-scan is essentially an  $x$ ,  $y$  plane at a selected value of  $Z$  or range of values of  $Z$ , many of the processes described in the previous section can be applied.

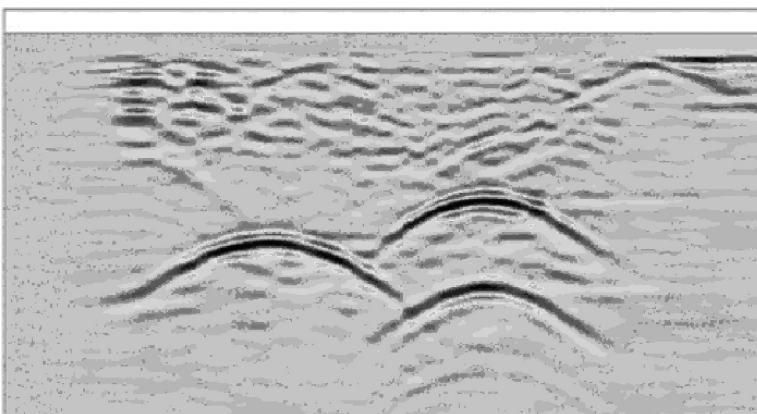


**FIGURE 21.27** B-scan data corrected for spreading loss and attenuation (*Courtesy IEE*)

Remembering that a GPR B-scan results in a hyperbolic cross section from a target, then an area scan (C-scan) will result in a hyperboloid of revolution whose vertical axis runs through the target. A plane orthogonal to the vertical axis will generate a circular feature whose radius increases with depth. A typical example is given in Figure 21.28, which shows the C-scans from an anti-tank mine buried at different depths with the center of the mine shown as an overlay. These images represent an unfocussed representation of the target as a result of the 3D spatial convolution of the antenna pattern with the target.

The variability of ground conditions, as well as the physics of EM wave propagation and reflection, must be carefully taken into account in attempting to classify targets even after image processing. For example, the depth image of a void is always apparently smaller than its physical size; corner reflectors of any reasonable size generate large apparently discontinuous reflection images; and conductive targets, which reverberate by means of stored energy, create extended depth images. The image of a buried target generated by a GPR will not, of course, correspond to its geometrical representation. The fundamental reasons for this are related to the ratio of the wavelength of the radiation and the physical dimensions of the target. In most cases for GPR, the ratio is close to unity. This compares very differently with an optical image, which is obtained with wavelengths such that the ratio is considerably greater than unity (typically 100,000:1). In GPR applications, the effect of combinations of scattering planes, for example, the corner reflector, can cause “bright spots” in the image, and variations in the velocity of propagation can cause dilation of the aspect ratio of the image. Although many images can be focused to reduce the effect of antenna beam spreading, regeneration of a geometric model is a much more complex procedure and is not usually attempted.

The general objective of signal processing as applied to GPR is to present either an image that can readily be interpreted by the operator or to classify the target return with respect to a known test procedure or template.

The general processing problem encountered in dealing with GPR data is in the widest sense the extraction of a localized wavelet function from a time series, which displays very similar time-domain characteristics to the wavelet. This time series is generated by signals from the ground and other reflecting surface, as well as internally from the radar system. Unlike conventional radar systems in which the target can generally be regarded as being in motion compared with the clutter, in the GPR case, the target and the clutter are spatially fixed and the radar antenna is moved with respect to the environment.

It is assumed that data are recorded to an adequate resolution. Most antennas used in surface penetrating applications have a limited low-frequency response and tend to act as high-pass filters effectively differentiating the applied impulse. As the ground acts as a low pass filter, the ground largely defines the bandwidth of reflected signal.

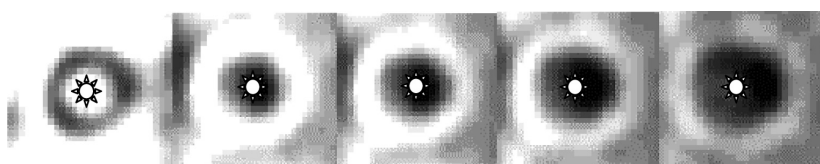


**FIGURE 21.28** Sequence of unfocussed C-scans of a set of a buried AT mine targets at depth increments of 10 mm (*Courtesy IEE*)

In the case of antennas operated in close proximity to the ground, the antenna characteristics may vary as a result of changes in the ground surface electrical parameters. Any processing scheme that assumes the antenna parameters remain constant needs to account for the mode of operation of the antennas and the degree of stability that is practically realizable. This is a particular issue for GPR and needs careful attention to reduce the effect of antenna-ground surface interaction.

Some of the ancillary requirements of an operational GPR system need to be considered. Accurate, high-resolution, low-cost position referencing systems for use with radar for subsurface survey techniques are now available. It is important that data can be related to a true geographic reference particularly when filed on digital mapping systems and used to define areas of safe working.

Another consideration is the plane of polarization of the electromagnetic energy. For targets with one large area dimension such as a pipe, the radar cross-scattering section will be larger when the polarization vector is in line with the pipe. This means that any area that is surveyed with, say, parallel dipoles must be surveyed in orthogonal directions to ensure that no targets are missed. The same requirement also relates to crossed dipole antennas.

## 21.9 APPLICATIONS

---

It is only possible to provide a brief summary of the wide variety of the applications for GPR, which has in some cases become an established and routine method of subsurface investigation. GPR, in the hands of an expert, provides a safe and noninvasive method of conducting speculative searches without the need for unnecessary disruption and excavation. A typical example of a GPR image is shown in Figure 21.29 with the various features identified.

GPR has significantly improved the efficiency of the exploratory work that is fundamental to the construction and civil engineering industries, the police and forensic sectors, security/intelligence forces, and archaeological surveys.

GPR has been very successfully used in forensic investigations. The most notorious case being in the United Kingdom in 1994, when the gravesites, under concrete and in the house of Fred West, of the victims of the serial murderer were pinpointed. In Belgium, the gravesites of the victims of the pedophile, Duteous, were detected in 1996.

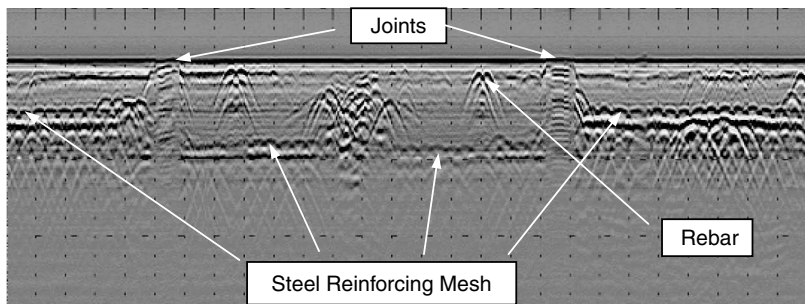


**FIGURE 21.29** Typical radar image of concrete floor showing rears, joints, mesh, etc: 1 ns pulse-width, horizontal markers every 10 cm, vertical scale 0.5 m (*Courtesy IEE*)



**FIGURE 21.30** Temple steps (*Courtesy IEE*)

Archaeological applications of GPR have been varied, ranging from the exploration of Egyptian and North American Indian sites as well as castles and monasteries in Europe. The quality of the radar image can be exceptionally good, although correct understanding normally requires joint interpretation by the archaeologists and radar specialists. Since 1990, the Square Geophysical Survey Project, under the auspices of the National Museum of Scotland and the Glasgow Museums, have been carrying out geophysical and archaeological surveys at Square in Egypt. Square forms part of the necropolis of the ancient Egyptian capital city of Memphis. The burial grounds extend from Abu Roash, just to the north of Cairo, southward through Giza, Abusir, Saqqara, and Dahshur to Meidum approximately 20 km to the south. The famous Step Pyramid of the 3rd Dynasty ruler, King Zoser, dominates the site of Saqqara. The main monument is known as the Gisr el-Mudir, which consists of a 400 meter east to west by 600 meter north to south stone enclosure. The walls are of extremely crude construction, but massive. This monument may constitute one of the oldest stone buildings in Egypt and hence the world. One of the main goals of the project has been to determine what, if anything, lies within the enclosure. Despite many years of surveying, nothing has been found apart from a small area of mud brick pavement. A number of radar sections had been measured over this area previously, and in view of the magnetometry results, the radar profiles were reexamined. The sections have been measured on 25 meter centers, so it was purely by chance that one radar survey line went straight down the flight of steps (excavated) seen in Figure 21.30 with the radar image in Figure 21.31.

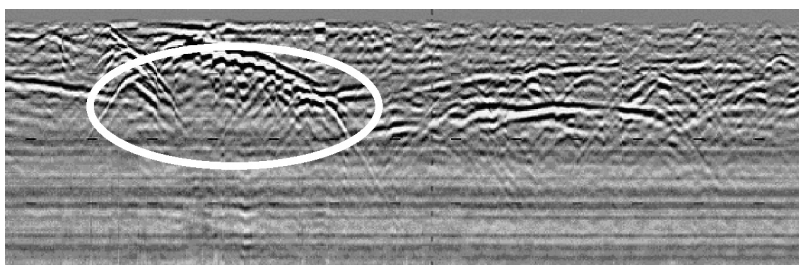


**FIGURE 21.31** Radar section along the flight of steps (*Courtesy IEE*)

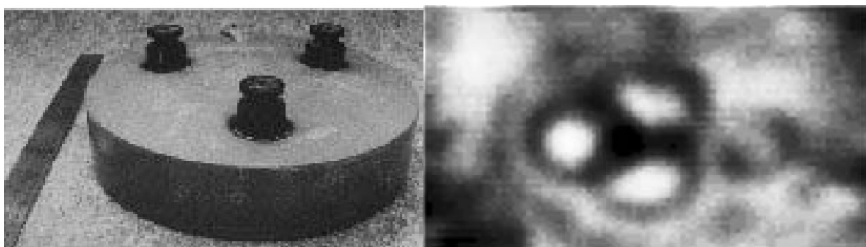


FIGURE 21.32 Example of GPR image of TMA3 AT mine (*Courtesy IEE*)

Abandoned antipersonnel land mines and unexploded ordnance are a major hindrance to the recovery of many countries from war. Their effect on the civilian population is disastrous and major efforts are being made by the international community to clear the problem. Most detection is done with metal detectors, which respond to the large amount of metallic debris in abandoned battlefield areas and hence have difficulty in detecting the minimum metal or plastic mine. GPR technology is being applied to this problem as a means of reducing the false alarm rate and providing improved detection of low-metal-content mines. Typical examples of radar images at various scales are shown in Figure 21.32 and Figure 21.33.

GPR has been used for surveying many different types of geological strata ranging from exploration of the Arctic and Antarctic icecaps and the permafrost regions of North America, to mapping of granite, limestone, marble, and other hard rocks as well as geophysical strata. The radar data shown in Figure 21.34 were collected at Finsterwalderbreen glacier, Svalbard, Norway, which is an island almost  $80^{\circ}$  north of Norway. The glacier is an 11 km long, land-terminated glacier with an area of 35 square km. The glacier depth starts at 30 meters and increases down to 250 meters. In the beginning of the profile, only the bottom echo is seen. At around 2 km horizontal distance, some internal scattering from the glacier is seen. This is scattering from the free water inside the glacier. From 4 km to 5 km, the bottom echo is difficult to see due to scattering.

The thickness of the various layers of a road can be measured using GPR techniques as shown in Figure 21.25. The great advantage is that this method is nondestructive and high speed ( $>40$  km/hr) and can be applied dynamically to achieve a continuous profile or rolling map. The accuracy of calibration tends to reduce as a function of

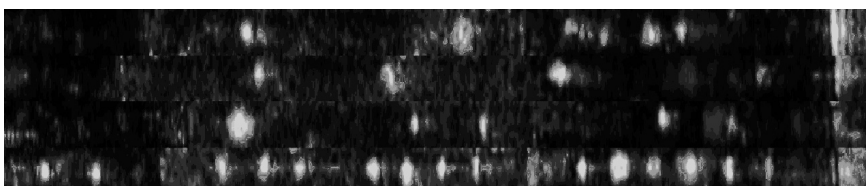
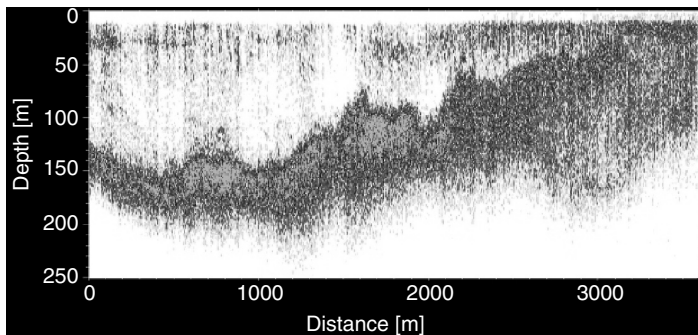
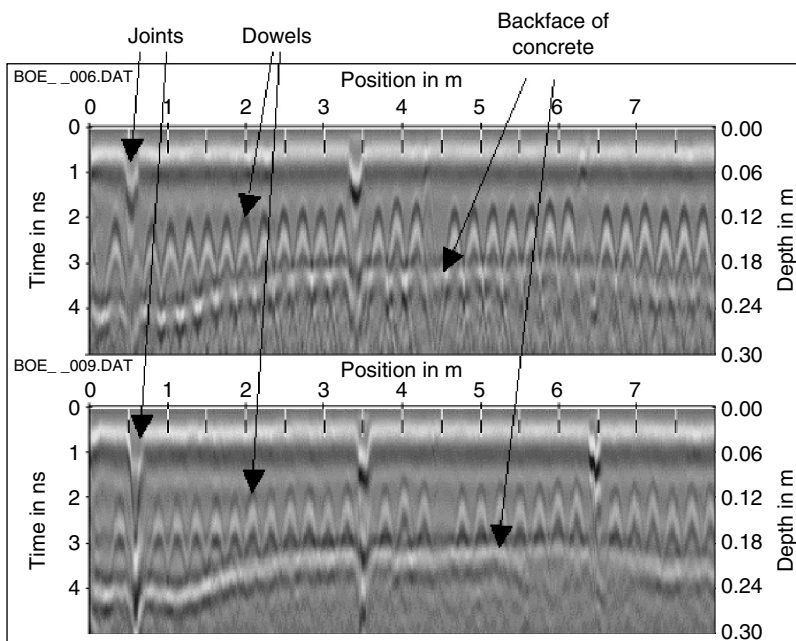


FIGURE 21.33 Example of AT mine images taken over a 4 m by 20 m test site with the MINDER GPR radar system (*Courtesy IEE*)



**FIGURE 21.34** Radar profiles along the centerline on Finsterwalderbreen glacier at 320–370 MHz (*from Hamran et al., 2000*)

depth because of the attenuation characteristics of the ground. The accuracy may be quite high (i.e., a few millimeters) for the surface-wearing course, but will reduce to centimeters at depths of one meter.



**FIGURE 21.35** Radar images using 1.5 GHz pulse duration along an 8-m long transversal trace close to a joint of a highway concrete deck. Top: Polarization parallel to the dowels; bottom: Polarization perpendicular to the dowels. (*Courtesy IEE*)

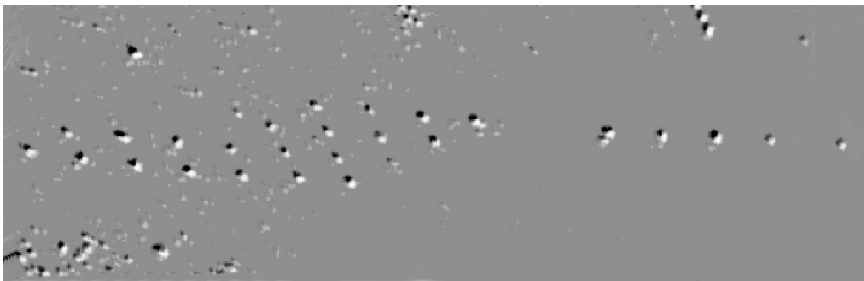


**FIGURE 21.36** UWB SAR image of buried AT mines in the Yuma Desert, aircraft at 400 m altitude  
(Courtesy SRI International USA, Dr. R. Vickers)

It has been shown that it is feasible to detect AT mines in dry soil conditions using airborne radar systems that operate over the frequency range 0.2–1 GHz. Figure 21.36 shows a radar image taken from an altitude of 400 meters above the Yuma desert. The radar operated at a depression angle of 45° and achieved a nominal resolution of 80 cm. It was capable of detecting metal AT mines of 30-cm diameter buried at a depth of 15–30 cm in a soil of conductivity 8–10 mmhos/m. Further details can be obtained from SRI International USA.

## 21.10 LICENSING

---

All countries require that GPR systems are properly regulated and operated in accordance with national and international requirements. Users should consult with their national authorities to determine the regulatory environment.

Within the European Union (EU), there are two main considerations governing the use of GPR. These are the use first of the equipment as a deliberate radio frequency radiator and second as an equipment that must satisfy the EMC requirements of the EU. The European Telecommunications Standards Institute (ETSI) regulatory body is in the process of drafting specifications and information can be found at <http://www.etsi.org> that will cover the use of such equipment as a deliberate radio frequency radiator. Legislation and an ETSI product specification means that this equipment will need to conform to the Radio & Telecommunications Terminal Equipment (R&TTE) — Directive. In the short term, until a new product specification is introduced and formally published in the Official Journal of the European Communities, the EMC Directive should be applied. All equipment, including ultrawideband radar or GPR, must be (Conformité Européene) CE marked to demonstrate that it satisfies the relevant directives of the European Union. The CE mark may only be applied when the requirements of all other relevant EU Directives, such as safety, have also been demonstrated. In the U.S. the FCC web site<sup>30</sup> provides current information and the limits are shown in Figure 21.37.

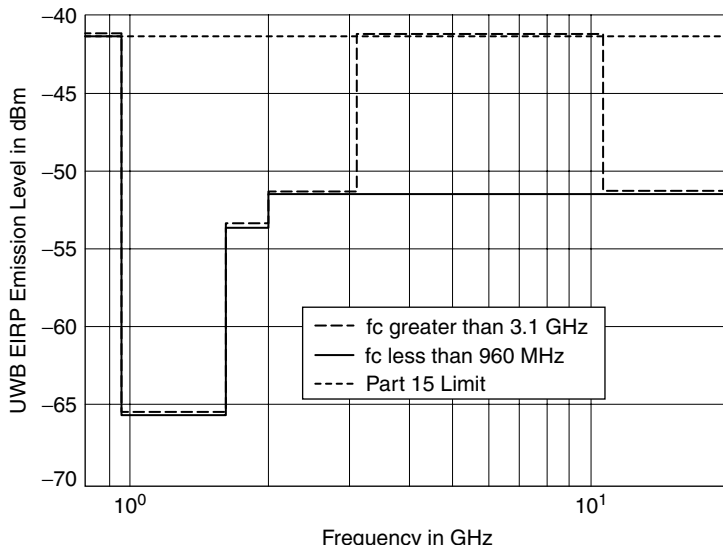


FIGURE 21.37 FCC emission limits

## REFERENCES

---

1. D. J. Daniels, *Ground Penetrating Radar*, 2nd Ed. IEE Radar Sonar Navigation and Avionics Series, London: IEE Books, July 2004.
2. B. O. Steenson, "Radar methods for the exploration of glaciers," Ph.D. dissertation, Calif. Inst. Tech., Pasadena, CA, 1951.
3. S. Evans, "Radio techniques for the measurement of ice thickness," *Polar Record*, vol. 11, pp. 406–410, 1963.
4. R. R. Unterberger, "Radar and sonar probing of salt," in *5th Int. Symp. on Salt*, Hamburg (Northern Ohio Geological Society), 1979, pp. 423–437.
5. R. M. Morey, "Continuous sub-surface profiling by impulse radar," in *Proc. Conf. Subsurface Exploration for Underground Excavation and Heavy Construction*, Amer. Soc. Civ. Eng., 1974, pp. 213–232.
6. P. K. Kadaba, "Penetration of 0.1 GHz to 1.5 GHz electromagnetic waves into the earth surface for remote sensing applications," in *Proc. IEEE S.E. Region 3 Conf*, 1976, pp. 48–50.
7. J. C. Cook, "Status of ground-probing radar and some recent experience," in *Proc. Conf. Subsurface Exploration for Underground Excavation and Heavy Construction*, Amer. Soc. Civ. Eng., 1974, pp. 175–194.
8. J. C. Cook, "Radar transparencies of mine and tunnel rocks," *Geophys.*, vol. 40, pp. 865–885, 1975.
9. K. C. Roe and D. A. Ellerbruch, "Development and testing of a microwave system to measure coal layer thickness up to 25 cm," Nat. Bur. Stds., Report No. SR-723-8-79 (Boulder, CO), 1979.
10. B. Nilsson, "Two topics in electromagnetic radiation field prospecting," Ph.D. dissertation, University of Lulea, Sweden, 1978.
11. D. J. Daniels, *Surface Penetrating Radar*, IEE Radar Sonar Navigation and Avionics Series 6, London: IEE Books, 1996.
12. See Reference 1.

13. Cook and Bernfeld, *Radar Signals, An Introduction to Theory and Application*, Norwood, MA: Artech House, p. 9.
14. M. Skolnik, *Radar Handbook*, 2nd Ed., New York: McGraw-Hill, 1990, Chap. 10.
15. F. Nathanson, *Radar Design Principles*, New York: McGraw-Hill, 1969, Chap. 8.
16. Wehner, *High Resolution Radar*, Chap 4.
17. Galati, *Advanced Radar Techniques and Systems*, IEE Radar Sonar Navigation and Avionics Series Vol. 4 London: IEE Books, 1993, p. 104.
18. Astanin and Kostylev, *Ultra-wideband Radar Measurements Systems*, IEE Radar Sonar Navigation and Avionics Series, Vol. 7, London: IEE Books, 1997, Chap. 1.
19. M. T. Tuley, J. M Ralston, F. S. Rotondo, A. M. Andrews, and AE. M. Rosen, "Evaluation of EarthRadar unexploded ordnance testing at Fort A.P. Hill, Virginia," *IEEE Aerospace and Electronics Systems Magazine*, vol. 17, issue 5, pp. 10–12, May 2002.
20. P. Debye, *Polar Molecules*, New York: Chemical Catalog Co., 1929.
21. K. S. Cole and R. S. Cole, "Dispersion and absorption in dielectrics, I, alternating current characteristics," *J. Phys. Chem.*, vol. 9, pp. 341–351, 1941.
22. D. J. Daniels, "Resolution of UWB signals," *IEE Proc. Radar Sonar and Navigation*, vol. 146, pp. 189–194, August 1999.
23. C. Martel, M. Philippakis, and D. J. Daniels, "Time domain design of a TEM horn antenna for GPR," presented at Millennium Conference on Antennas and Propagation, April 2000.
24. D. J. Daniels, "An assessment of the fundamental performance of GPR against buried landmines," presented at SPIE Detection and Remediation Technologies for Mines and Minelike Targets XII, Orlando, FL, April 2007
25. G. Denniss "Solid-state linear FMCW systems –their promise and their problems," in *Proc. IEEE Int. Mic. Conf.*, Atlanta, GA, 1974, pp. 340–345.
26. R. M. Narayanan, Y. Xu, P. D. Hoffmeyer, and J. O. Curtis, "Design, performance, and applications of a coherent random noise radar," *Optical Engineering*, 37(6), pp. 1855–1869, June 1998.
27. J. Sachs, P. Peyerl, F. Tkac, and M. Kmec, "Digital ultra-wideband-sensor electronics integrated in SiGe-technology," in *Proc. of the EuMC*, vol. II, Milan, Italy, September 2002, pp. 539–542.
28. J. Sachs and P. Peyerl, "Chip integrated UWB radar electronics," presented at Third DTIF Workshop, *Ground Penetrating Radar in Support of Humanitarian Demining*, JRC, Ispra, Italy, September 2002.
29. J. R. Wait, "Propagation of electromagnetic pulses in a homogeneous conducting earth," *Appl. Sci. Res. B*, vol. 8, pp. 213–253, 1960.
30. R. W. P. King and T. T. Nu, "The propagation of a radar pulse in sea water," *J. Appl. Phys.*, 73, (4), pp. 1581–1589, 1993.
31. D. B. Rutledge and M. S. Muha, "Imaging antenna arrays," *IEEE Trans*, AP130, (Q), pp. 533–540, 1982.
32. Federal Communications Commission, <http://www.fcc.gov/aboutus.html>.

